Astronomy & Astrophysics manuscript no. main
October 15, 2025

A constant upper luminosity limit of cool supergiant stars down to the extremely low metallicity of I Zw 18

Abel Schootemeijer[1], Ylva Götberg[2], Norbert Langer[1,3], Giacomo Bortolini[4], Alec S. Hirschauer[5], and Lee Patrick[6]

[1] Argelander-Institut für Astronomie, Universität Bonn, Auf dem Hügel 71, 53121 Bonn, Germany
e-mail: aschoot@astro.uni-bonn.de
[2] Institute of Science and Technology Austria (ISTA), Am Campus 1, 3400 Klosterneuburg, Austria
[3] Max-Planck-Institut für Radioastronomie, Auf dem Hügel 69, 53121 Bonn, Germany
[4] Department of Astronomy, The Oskar Klein Centre, Stockholm University, AlbaNova, 10691 Stockholm, Sweden
[5] Department of Physics & Engineering Physics, Morgan State University, 1700 East Cold Spring Lane, Baltimore, MD 21251, USA
[6] Centro de Astrobiología (CSIC-INTA), Ctra. Torrejón a Ajalvir km 4, 28850 Torrejón de Ardoz, Spain

Preprint online version: October 15, 2025

ABSTRACT

Stellar wind mass loss of massive stars is often assumed to depend on their metallicity Z. Therefore, evolutionary models predict that massive stars in lower-Z environments are able to retain more of their hydrogen-rich layers and evolve into brighter cool supergiants (cool SGs; $T_{\rm eff} < 7\,$kK). Surprisingly, in galaxies in the metallicity range $0.2 \lesssim Z/Z_\odot \lesssim 1.5$ previous studies did not find a metallicity dependence of the upper luminosity limit $L_{\rm max}$ of cool SGs. Here, we add four galaxies to the sample studied for this purpose with data from the Hubble Space Telescope and the James Webb Space Telescope (JWST). Observations of the extremely metal-poor dwarf galaxy I Zw 18 from JWST allow us to extend the studied metallicity range down to $Z/Z_\odot \approx 1/40$. For cool SGs in all studied galaxies including I Zw 18, we find a constant value of $L_{\rm max} \approx 10^{5.6}\,{\rm L}_\odot$, similar to literature results for $0.2 \lesssim Z/Z_\odot \lesssim 1.5$. In I Zw 18 and the other studied galaxies, the presence of Wolf-Rayet stars has been inferred previously. Although we cannot rule out that some of them become intermediate-temperature objects, this paints a picture in which evolved stars with $L > 10^{5.6}\,{\rm L}_\odot$ burn helium as hot helium-rich stars down to extremely low metallicity. We argue that metallicity-independent late-phase mass loss would be the most likely mechanism responsible for this. Regardless of the exact stripping mechanism (winds or e.g. binary interaction), for the Early Universe our results imply a limitation on black hole masses and a contribution of stars born with $M \gtrsim 30\,{\rm M}_\odot$ to its surprisingly strong nitrogen enrichment. We propose a scenario in which single stars at low metallicity emit sufficiently hard ionizing radiation to produce lines of He II and C IV. In this scenario, late-phase metallicity-independent mass loss produces hot helium-rich stars. Due to the well-understood metallicity dependence of radiation-driven winds of hot stars, a window of opportunity would open below $0.2\,{\rm Z}_\odot$, where self-stripped helium-rich stars can exist without dense WR winds that absorb hard ionizing radiation.

Key words. Stars – red supergiants – Stars: winds – Stars: black holes

1. Introduction

At the end of their lives, massive stars in the Early Universe might or might not be able to retain their hydrogen-rich outer layers. If they are destined to lose these layers, they are expected to evolve into hot helium-rich stars. These stars emit copious amounts of high-energy photons (Todt et al. 2015; Kubátová et al. 2019), which would contribute to the ionization of their surroundings. This might help to explain observed signatures of ionizing radiation of, for example, He II and C IV emission observed in galaxies from low to high redshifts (Stark et al. 2015; Senchyna et al. 2019; Saxena et al. 2020; Mingozzi et al. 2022, 2024; Hayes et al. 2025). Current stellar population synthesis models tend to produce too little of this ionizing radiation, which is why recent works often resort to blackbody models to explain observations (Olivier et al. 2022; Cameron et al. 2024). If winds of hot helium-rich stars are dense, most of this ionizing radiation cannot escape (Sander & Vink 2020). Such dense winds can give rise to strong emission lines in stellar spectra. Stars showing this emission are classified as Wolf-Rayet (WR) stars, which can affect their host galaxy's spectral appearance (Conti & Vacca 1994) and evolution (Crowther 2007).

It is sometimes assumed that the hydrogen-rich layers of stars born more massive than $\sim 35\,{\rm M}_\odot$ fall back into a black hole (BH) after their supernova explosion (Fryer et al. 2012), although this is not certain (Lovegrove & Woosley 2013; Costa et al. 2021). If the fallback scenario is true, loss of hydrogen-rich layers before the supernova reduces the masses of BHs that massive stars can produce. Since BH masses can be measured from gravitational merger events (Abbott et al. 2016), a redshift-dependence of BH masses could be expected if this mass loss is metallicity dependent. So far no evidence of such a dependence has been found up to a redshift of one (Lalleman et al. 2025), but future high-sensitivity measurements could provide further insight.

Unfortunately, for galaxies in the Early Universe, detailed studies of the individual stars and their mass loss remain impossible. Fortunately, clues can be found by investigating, for example, red supergiants (RSGs; stars with thick hydrogen envelopes) in nearby galaxies that are also metal-poor. In the sample studied for this purpose, which includes the Large Magellanic Cloud (LMC), the Small Magellanic Cloud (SMC), M 31, and the Milky Way (MW) itself, RSGs exist only up to a luminosity limit of $\log(L/L_\odot) \approx 5.6$, which corresponds to an initial mass of $\sim 30\,{\rm M}_\odot$ (Brott et al. 2011; Georgy et al. 2013). This so-called Humphreys-Davidson limit seems to be independent of metallicity – at least down to the metallicity of the SMC where $Z = 1/5\,Z_\odot$ (Humphreys & Davidson 1979, 1994; Davies et al. 2018; McDonald et al. 2022; de Wit et al. 2024; Bonanos 2025).

In the same galaxies, a multitude of hot WR stars (which no longer have thick hydrogen envelopes) have been found to exist at luminosities of $\log(L/L_\odot) > 5.6$; see for example Rate & Crowther (2020) for the Milky Way, Hainich et al. (2014, 2015); Shenar et al. (2016, 2019) for the Magellanic Clouds, and Sander et al. (2014); Neugent & Massey (2023) for M 31. Together, the luminosity properties of WR stars and RSGs paint a picture in which stars that have metallicities down to $Z = 1/5\,Z_\odot$ and initial masses of $M_{ini} \gtrsim 30\,M_\odot$ lose their hydrogen-rich layers and evolve into WR stars.

Given that wind mass loss rates of hot stars depend on metallicity (Mokiem et al. 2007; Hainich et al. 2015; Backs et al. 2024), this lack of metallicity dependence of the RSG luminosity limit has been a long-standing puzzle. It could imply that mass loss of cooler evolved stars is strong at low metallicity (e.g., Lamers & Fitzpatrick 1988; Yang et al. 2023; Schootemeijer et al. 2024). It could also be that internal mixing (Schootemeijer et al. 2019; Higgins & Vink 2020; Gilkis et al. 2021; Sabhahit et al. 2021) and/or binary stripping (Paczyński 1967; Vanbeveren & Conti 1980; Pauli et al. 2022a) play an important role.

Here, we aim to further investigate the upper luminosity limit of stars that can retain their hydrogen-rich envelopes. We expand the sample of galaxies studied for this purpose using archival data from the Hubble Space Telescope (HST), and, importantly, extend the explored metallicity range down to $1/40\,Z_\odot$ with new observations of I Zw 18 (Hirschauer et al. 2024; Bortolini et al. 2024) taken with the James Webb Space Telescope (JWST). We structure our paper as follows. We discuss observational data of the dwarf galaxies that we investigate in Sect. 2. In Sect. 3 we discuss our methods, and in Sect. 4 we show our results. Finally, we discuss possible caveats and the implications of our results in Sect. 5, and we present our conclusions in Sect. 6.

2. Data of target galaxies

In this study, we make use of a variety of archival photometry data. Infrared (IR) observations of I Zw 18 were taken with JWST (see Hirschauer et al. 2024). From these data, Bortolini et al. (2024) performed point source extraction and aperture photometry using the software package DOLPHOT (Dolphin 2000; Weisz et al. 2024). Here we use this catalog from Bortolini et al. (2024), adopting the same source selection criteria (e.g., for signal-to-noise) as described there. From this data set, we use the data obtained with the $F115W$ and $F200W$ filters. To test our method, we also use optical HST data of I Zw 18 from Aloisi et al. (2007), which were transformed to V and I magnitudes by these authors.

To expand our sample of dwarf galaxies, we search the data archives of the ACS Nearby Galaxy Survey Treasury (ANGST; Dalcanton et al. 2009) and the Legacy ExtraGalactic UV Survey (LEGUS; Sabbi et al. 2018). From these data archives, we select galaxies by eye that appear to have a well-populated RSG branch: NGC 300, NGC 3109, NGC 55, and Sextans A from ANGST and NGC 5253, NGC 4395, and Ho II from LEGUS. Further inspection of the data showed that NGC 3109, NGC 55, Sextans A, and Ho II have about an order of magnitude fewer bright red sources than the other three dwarf galaxies (and the brightest sources are relatively dim). This is line with their relatively small amount of bright main-sequence stars. Therefore, we discard those galaxies, as they are less useful for drawing statistically significant conclusions. The sample of dwarf galaxies from ANGST and LEGUS that we include in the end is thus NGC 300, NGC 5253, and NGC 4395.

We do not include the Milky Way, because its individual stars can suffer from uncertain distances, which would propagate into uncertain luminosities. We do include previous studies that calculated RSGs luminosities in the SMC and LMC (Davies et al. 2018) and M 31 (McDonald et al. 2022). We compile properties of the galaxies in our final sample in Table 1. These include the distance modulus (DM) and distance, the average visual extinction A_V, and the metallicity. These galaxies cover a metallicity range of $1/40 \lesssim Z/Z_\odot \lesssim 1.5$.

Table 1. Properties of our target galaxies.

Galaxy	DM [mag]	Distance [Mpc]	A_V [mag]	Z [$Z_\odot$]	Lref[1]
I Zw 18	31.3 [a)]	18.2	0.1 [b)]	1/40 [c)]	TW
SMC	18.977 [d)]	0.062	0.35 [e)]	1/5 [f)]	[g)], TW
NGC 5253	27.48 [h)]	3.1	0.3 [i)]	1/3 [j)]	TW
NGC 300	27.36 [k)]	3.0	0.15 [l)]	1/2.5 [m)]	TW
LMC	18.476 [n)]	0.050	(not used)	1/2 [o)]	[g)]
NGC 4395	28.15 [p)]	4.3	0.3 [q)]	1 [r)]	TW
M 31	24.407 [s)]	0.761	(not used)	1.5 [t)]	[u)]

Notes. [1]: Lref is the reference to the work in which cool SG luminosities are measured, where TW is this work. References: [a)]: Aloisi et al. (2007) – [b)]: Izotov & Thuan (2016), Hirschauer et al. (2024) – [c)]: from Lebouteiller et al. (2013) and from oxygen abundances of Skillman & Kennicutt (1993) compared to $\log(O/H)_\odot = 8.75$ (Bergemann et al. 2021) – [d)]: Graczyk et al. (2020) – [e)]: Schootemeijer et al. (2021) – [f)]: Venn (1999) – [g)]: Davies et al. (2018) – [h)]: Davidge (2007) – [i)]: Abril-Melgarejo et al. (2024) – [j)]: Monreal-Ibero et al. (2012) – [k)]: Rizzi et al. (2006) – [l)] Micheva et al. (2022) – [m)]: Gazak et al. (2015) – [n)]: Pietrzyński et al. (2019) – [o)]: Davies et al. (2015), Patrick et al. (2016), Choudhury et al. (2021) – [p)]: Thim et al. (2004) – [q)]: based on $A_{263\,nm} \approx 0.75$ (Nandi et al. 2023) and A_λ/A_V from Gordon et al. (2003) – [r)]: Cedrés & Cepa (2002) – [s)]: Li et al. (2021) – [t)]: based on Zaritsky et al. (1994) and Bergemann et al. (2021) – [u)]: McDonald et al. (2022).

3. Methods

3.1. Identifying cool supergiants

Often, RSGs are selected with cuts in color-magnitude diagrams (CMDs). The use of CMD cuts to classify sources in different target galaxies is hindered by three issues that cause systematic shifts: i), different extinction values, ii), the use of different filters (e.g., $F606W - F814W$ color instead of $F555W - F814W$), and, iii), different metallicities, which lead to different effective temperatures. Therefore, we trained a neural network (NN) on SMC data to identify RSGs, as we describe below. We start with the source catalog of Yang et al. (2019), who have combined a plethora of photometric data of evolved SMC stars. From this catalog, we use *2MASS* (Skrutskie et al. 2006) and *Skymapper* (data release 1.1; Wolf et al. 2018) data (Fig. 1). Specifically, we use cuts in an IR CMD constructed with 2MASS J and K_S data to identify RSGs: the cut to separate RSGs and asymptotic giant branch (AGB) stars is adopted from Cioni et al. (2006), and for RSGs we also adopt $M_{K_S} < -5.8$ and $J - K_S > 0.6$ (see top left panel of Fig. 1).

We applied a 70-30 train-test split to the SMC sample. Next, we plotted the RSG and non-RSG sources from the training set in an $r - i$ CMD using the *Skymapper* data. Then we used the KERAS TENSORFLOW library (TensorFlow Developers 2022) to

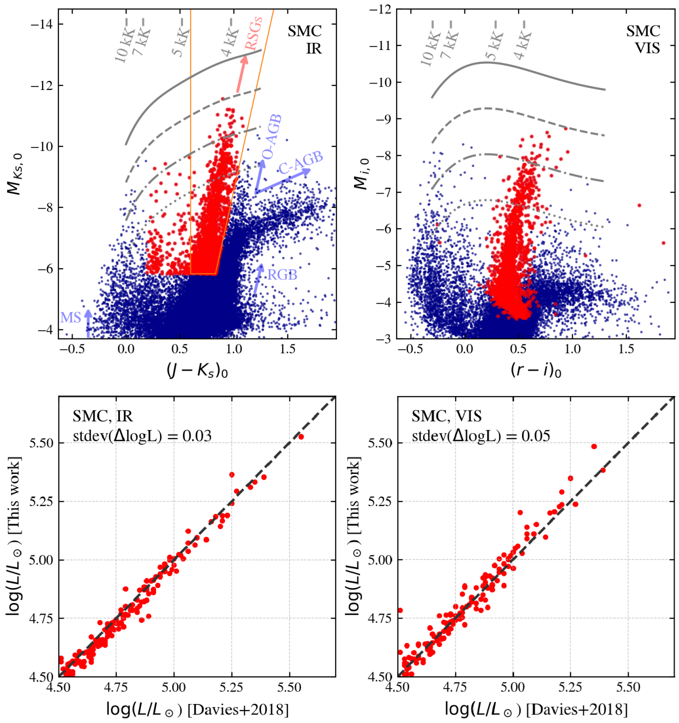

Fig. 1. *Top panels:* extinction-corrected color-magnitude diagrams of SMC sources, based on IR data (left) and optical 'VIS' data (right). Orange lines show the RSG cuts in the IR. Red markers indicate sources that we classified as cool SGs, and blue markers indicate other sources. The four grey lines are iso-luminosity lines (Eq. 2). These iso-luminosity lines represent $\log(L/L_\odot)$ = 6.0, 5.5, 5.0, and 4.5, where the higher values are closer towards the top of the plots. At the top of each panel, gray ticks at various colors are labeled by the temperatures to which they correspond according to the adopted bolometric corrections. In the top left panel, following Nally et al. (2024), the arrows parallel to various features indicate the main sequence (MS), red giant branch (RGB), oxygen (O) and carbon (C) AGB, and the RSGs. *Bottom panels:* luminosities calculated in this work (both in the visual as in the infrared) as a function of luminosities calculated in earlier work by Davies et al. (2018). The dashed black line indicates where both luminosities would be identical.

build a NN with two hidden layers of 16 units each. The upper hidden layer used a 'relu' activation function, and the lower hidden layer and the output layer used a 'sigmoid' activation function. This NN was trained to identify RSGs and non-RSGs based on their position in the $r - i$ CMD. Here we chose the r and i filters because they transmit light at similar wavelenghts as the $F555W$ and $F814W$ HST filters that we will consider later on. We applied the NN to the test data to confirm that it properly identified RSGs.

The trained and tested NN was then used to identify RSGs in the optical CMDs of NGC 5253, NGC 300, and NGC 4395, which were compiled with optical HST data. Later on, we will compare with models that have temperatures up to 7 kK. Therefore, we extend the color range in the CMDs down to 0.25. Because that includes not only RSGs but also yellow supergiants, we will hereafter refer to the stars selected by the NN and extended color range as 'cool SGs'. For the purpose of this study, the crucial aspect of the cool SG selection method is that it includes the highest-luminosity sources. This is the case, as is demonstrated by the CMDs with highlighted cool SGs (top panels of Fig. 1 and Fig. 2). The cool SG selection method might perform suboptimally at $M_{abs} \gtrsim -6$, where it appears to include some AGB stars. However, this is not a concern for our analysis later on, where we include only sources at $\log(L/L_\odot) \geq 4.6$.

Two sources near the $\log(L/L_\odot) = 6$ line in NGC 4395 were also initially classified as cool SGs. These sources are bright enough to have astrometric measurements in the Gaia DR3 catalog[1] (Gaia Collaboration et al. 2023), which indicate that they are foreground sources (e.g., proper motions in the declination direction of $pm_{dec} = 0.96 \pm 0.11$ and $pm_{dec} = 6.67 \pm 0.12$, while we expect proper motions consistent with zero at the distance of 4.3 Mpc). Therefore, we do not consider these two sources as bright cool SGs in further analysis.

We note that in the optical SMC CMD, we found a few very red sources (with $(r - i)_0 > 1$) classified as cool SGs. Inspection of the data showed that they are not particularly bright in the K_S band, which argues against them being intrinsically very luminous sources suffering from high extinction.

In I Zw 18, which has a far lower metallicity ($\sim$1/40 $Z_\odot$) than the other galaxies in our sample, there is no well-defined RSG branch. This is likely a stellar evolution effect, as we will discuss in more detail later on. Because of this, we cannot apply the NN to identify cool SGs in I Zw 18. Instead, as an alternative method, we use evolutionary tracks of 8 $M_\odot$ with [Fe/H] = -1.7 from MIST[2] (Dotter 2016; Choi et al. 2016) to select evolved sources more massive than 8 $M_\odot$ (purple lines in bottom panels of Fig. 2 – these are evolved to near carbon exhaustion). For sources that are at redder colors, we extrapolate the tracks. Again, we exclude sources with a color bluer than 0.25 mag. As a test, we also applied this method involving MIST tracks to identify cool SGs in NGC 4395, NGC 5253, and NGC 300. Compared to the NN method, we identified marginally more sources as cool SGs at $4.5 < \log(L/L_\odot) < 5.0$, and, most importantly, we identified the same sources as cool SGs above $\log(L/L_\odot) = 5.0$ (our region of interest; Sect 4.2).

3.2. Calculating luminosities

To convert the colors and magnitudes from photometric observations into effective temperatures and luminosities, we used bolometric correction (BC) tables from MIST (Dotter 2016; Choi et al. 2016). To start, we selected effective temperatures in the range $3 \leq T_{eff}/\mathrm{kK} \leq 10$, a surface gravity of $\log(g\,\mathrm{cm}^{-1}\,\mathrm{s}^2)) = 0$, and metallicities that lie closest to the values shown in Table 1 (e.g., [Fe/H] = −0.75 for the SMC). We then fitted fifth-order polynomials to obtain T_{eff}-color relations at the relevant metallicities. We obtained color-BC relations (e.g., a relation between intrinsic $F115W - F200W$ color and BC_{F200W}) in a similar fashion. This allowed us to calculate the luminosity as follows:

$$\log(L/L_\odot) = -0.4\Big(M_{abs,0} - M_{bol,\odot} + BC(\mathrm{color})\Big). \quad (1)$$

Here, $M_{abs,0} = m_\lambda - DM - A_\lambda$ is the intrinsic absolute magnitude of a source, obtained from the apparent magnitude m_λ in the reddest filter used to construct the CMD, the distance modulus DM, and the extinction $A_\lambda = A_V \cdot A_\lambda/A_V$. The values used for DM and A_V are those shown in Table 1 and A_λ/A_V is from Wang & Chen (2019). We adopt $M_{bol,\odot} = 4.74$ for the Solar absolute bolometric magnitude.

[1] https://gea.esac.esa.int/archive/
[2] https://waps.cfa.harvard.edu/MIST/

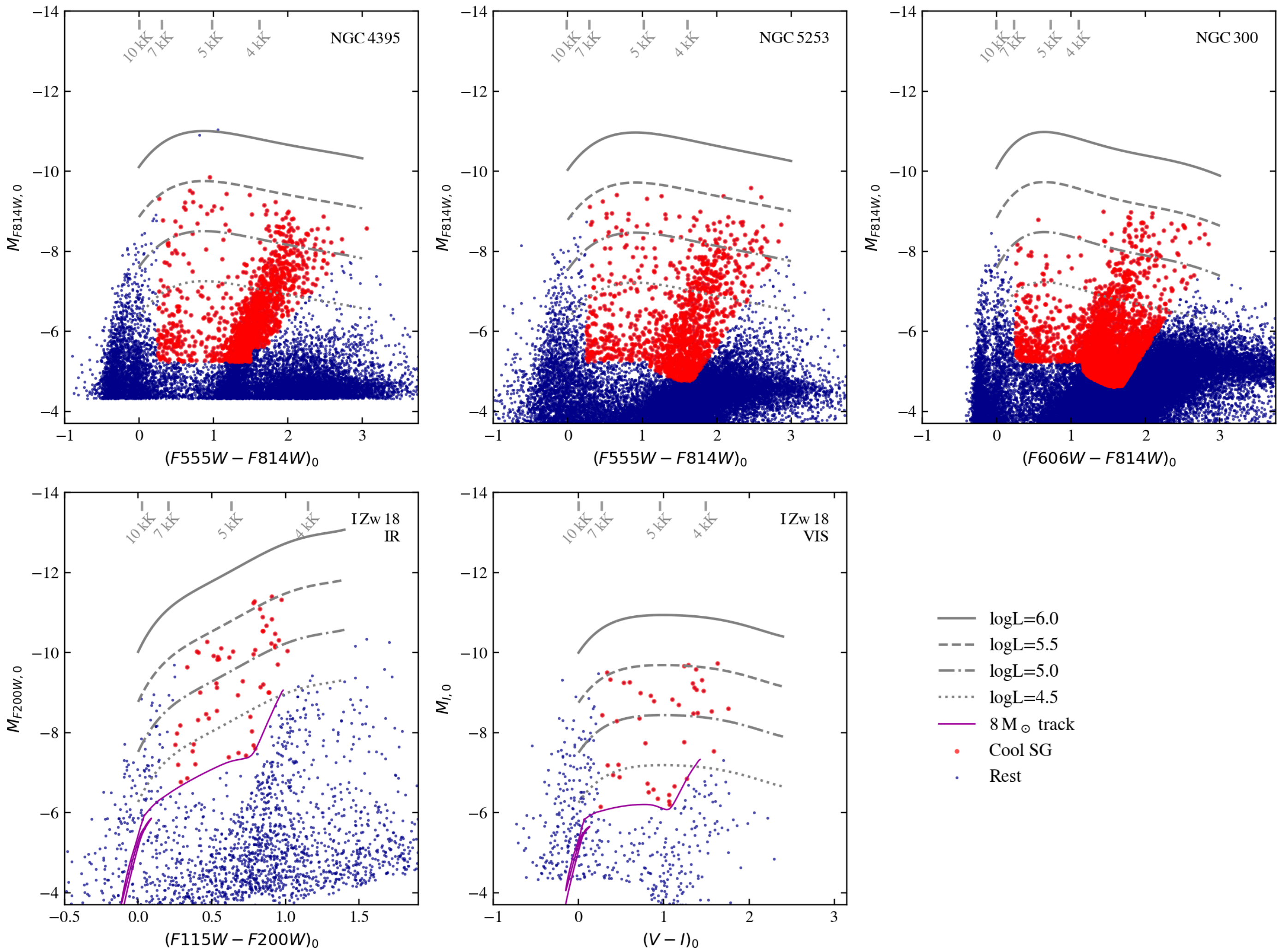

Fig. 2. Same as the top panels of Fig. 1, but for VIS data of NGC 4395, NGC 5253, and NGC 300 (*top panels*) and IR and VIS data of I Zw 18 (*bottom panels*). Also, the purple line in the bottom panels represents an 8 M$_\odot$ MIST track with [Fe/H] = -1.75.)

Similarly, we drew iso-luminosity lines in our CMDs (Figs. 1, 2). We calculated these using:

$$M_{\mathrm{abs},0}(\mathrm{color}) = -2.5\log(L/L_\odot) + M_{\mathrm{bol},\odot} - BC(\mathrm{color}). \quad (2)$$

For infrared (IR) and visible (VIS) data, we tested our method with SMC data from Davies et al. (2018), who have used photometry to calculate luminosities of cool SGs in the SMC by integrating over their spectral energy distributions. The catalog of Davies et al. (2018) provides *2MASS* IR photometry. To obtain VIS photometry we used CDS-xmatch[3] to cross-correlate the Davies et al. (2018) catalog with the catalog from Yang et al. (2019), which includes *SkyMapper* photometry. Figure 1 shows the correlation between the luminosity calculated by Davies et al. (2018) and by our method. The black line shows where the values would be equal (i.e., it is not a linear fit). The standard deviation of the difference in $\log(L/L_\odot)$ is 0.05 in the optical and 0.03 in the IR. We conclude that our method appears to accurately calculate cool SG luminosities, especially with IR data.

[3] http://cdsxmatch.u-strasbg.fr/

4. Results

4.1. Color-magnitude diagrams

We present optical CMDs of NGC 4395, NGC 5253, and NGC 300 in the top row of Fig. 2. Using the iso-luminosity lines for navigation, it is visible that the cool SGs in these galaxies are abundant up to $\log(L/L_\odot) \approx 5.6$, but absent at higher luminosities. In the bottom left panel of Fig. 2, we show the IR CMD of I Zw 18 based on JWST data (Hirschauer et al. 2024; Bortolini et al. 2024). At the bright end, the IR CMD shows the same behavior as the higher-metallicity galaxies, with cool SGs being present up to $\log(L/L_\odot) \approx 5.6$. We will discuss these luminosity distributions in more detail in Sect 4.2.

I Zw 18 is the most challenging of our target galaxies to study because it is the most distant. Therefore, we use optical data from Aloisi et al. (2007) to perform an independent measurement of the luminosities of cool SGs in I Zw 18 (lower central panel of Fig. 2). With the optical data we find that the brightest RSG has a luminosity of $\log(L/L_\odot) = 5.59$. With the IR data we obtained almost the same luminosity for the brightest RSG ($\log(L/L_\odot) = 5.57$); a difference of only 0.02 dex. We find this result encouraging.

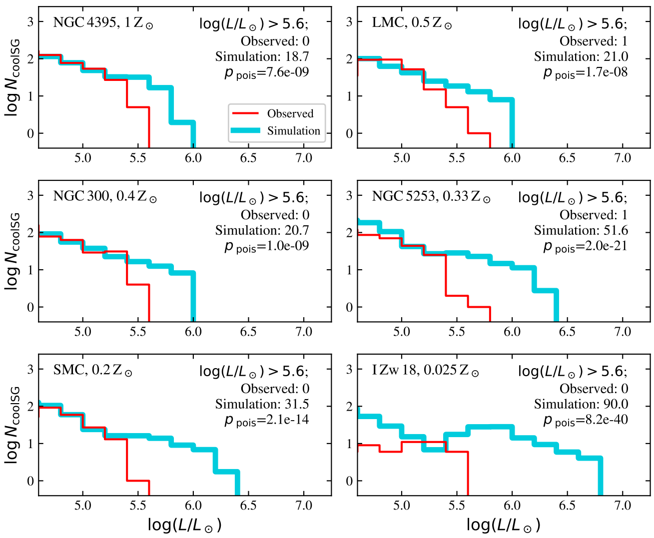

Fig. 3. Luminosity distributions of observed sources (red lines) and sources in the theoretical population (light blue lines) in six different galaxies. The observed SMC and LMC sources are taken from Davies et al. (2018), the rest is from this work. At the right side of each panel, we write the number of observed and model population sources with $\log(L/L_{\odot}) > 5.6$, and the associated Poisson probability to have as many observed sources or fewer (given the number of theoretically predicted sources).

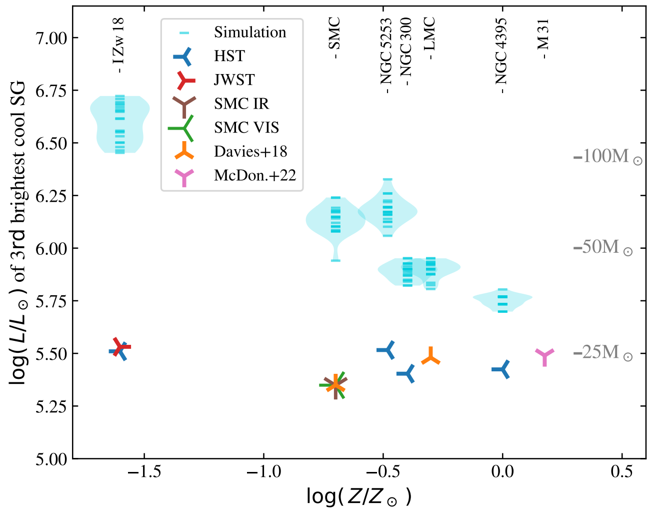

Fig. 4. Third brightest cool SG in various galaxies as a function of galaxy metallicity. The data points with the labels HST, JWST, SMC IR, and SMC VIS are from this work. The data points labeled Davies+18 and McDon+22 are based on the work of Davies et al. (2018) on the SMC and LMC, and the work of McDonald et al. (2022) on M 31, respectively. We note that I Zw 18 and the SMC have multiple data points that are similar within 0.02 dex. The light blue horizontal lines show the third brightest cool SG in individual simulations. We perform 20 simulations per galaxy, and we visualize the number density of the outcomes of the simulation with violin plots. The grey ticks indicate the time-averaged cool SG luminosities of BoOST SMC models with three different initial masses, which are similar across the shown metallicity range.

4.2. Luminosity distributions

In Fig. 3, we show the observed luminosity distributions (red lines) of cool SGs in the galaxies discussed in the previous section. For I Zw 18, we consider the luminosities based on the IR observations from JWST. Additionally, we include the LMC and the SMC, for which we obtain the cool SG luminosities directly from Davies et al. (2018).

For each galaxy, we compare this observed luminosity distribution with a model population from BoOST (Bonn Optimized Stellar Tracks; Szécsi et al. 2022). These BoOST models include moderate rotation and metallicity-dependent mass loss. They are an extension of the massive star model grid of Brott et al. (2011). We pick the closest-metallicty models for galaxies that have no models tailored for them: SMC models for NGC 5253, LMC models for NGC 300, and MW models for NGC 4395. We then draw random ages and random initial masses, where the probability for the initial mass is dictated by the Salpeter IMF ($p \propto M_{\rm ini}^{-2.35}$; Salpeter 1955). Then we discard a model if it has $T_{\rm eff} > 7$ kK and we discard models that have a stellar lifetime that is shorter than the drawn age. To reduce the statistical noise, we have given each drawn stellar model a weight of 0.05. We continue drawing random models until we have drawn the same number as observed in the luminosity range $5.0 \leq \log(L/L_{\odot}) \leq 5.4$ (e.g., if 20 such sources are observed, we keep drawing until we have 400 theoretical models with a statistical weight of 0.05 each). We tabulate numbers of observed and predicted cool SGs in Table A.1. There, we also provide a minimum SFR per galaxy based on its number of observed cool SGs ('minimum' because stars can burn helium also as hotter objects) – see Appendix A for details.

Comparing the observed and theoretical luminosity distributions, we find very good agreement below $\log(L/L_{\odot}) = 5.4$ (except for I Zw 18). Above $\log(L/L_{\odot}) = 5.6$, in the theoretical distribution there are far more models present than what is observed. The theoretical upper luminosity limits are in practice set by the adopted mass-loss rates, which are lower at low metallicity. Therefore, the tension with the (nearly constant) observed upper luminosity limit significantly increases with decreasing metallicity. At the right side of each panel of Fig. 3, we write the Poisson probability $p_{\rm pois}$ to draw as many or fewer cool SGs as are observed above $\log(L/L_{\odot}) = 5.6$, given the number that is expected from the theory population. For all galaxies, these Poisson probabilities are below 10^{-7}, meaning that the absence of observed cool SGs with $\log(L/L_{\odot}) > 5.6$ cannot plausibly be explained by chance.

We discuss the case of I Zw 18 in more detail. This is the only galaxy where the observed and theoretical luminosity distributions do not match at the low-luminosity end. The number of observed cool SGs in the range $4.6 < \log(L/L_{\odot}) < 5.0$ (corresponding to $M_{\rm ini} \approx 15\,{\rm M}_{\odot}$) is about five times lower than the models predict. We suspect that this could be a stellar evolution effect. In this scenario, stars born with $\sim$15 $M_{\odot}$ spend a smaller fraction of their helium-burning lifetime as cool SGs than stars with initial masses of $\sim$25 $M_{\odot}$ (which have $\log(L/L_{\odot}) \approx 5.4$ during helium burning). In fact, such a stellar evolution effect is present in the BOoST models, but higher luminosity (it causes the bump around $\log(L/L_{\odot}) \approx 5.8$ in the bottom right panel of Fig. 3). We will discuss uncertainties in stellar evolution models in Sect. 5.2. Because of these uncertainties, we used BoOST models to perform a test where we assumed that all I Zw 18 stars spend a constant fraction of 7% of their lifetime burning helium as cool SGs. This resulted in a model population harboring ∼10 cool SGs with $\log(L/L_\odot) > 5.6$, and an associated $p_{pois} \approx 10^{-4}$ to draw none. As such, in this test there is a less spectacular difference between the luminosity distributions of observed and model populations of bright cool SGs in I Zw 18. Still, the absence of observed cool SGs with $\log(L/L_\odot) > 5.6$ would again be very unlikely to be explained by chance.

4.3. Trend with metallicity

After calculating luminosity distributions of cool SGs in different galaxies, we now investigate possible trends with metallicity. To do so, we consider the third brightest observed cool SG in each galaxy, and plot it against the metallicity of its galaxy. We chose to take the third brightest object because one uncertain object can significantly scatter the upper luminosity limit (see e.g. the cases of McDonald et al. (2022) in M31, and the rapidly-changing object WOH G64 (Levesque et al. 2009; Davies et al. 2018; Ohnaka et al. 2024; Munoz-Sanchez et al. 2024) in the LMC). Our conclusions would be the same when considering the brightest cool SG instead of the third brightest. We note that we included only RSGs from literature studies of the SMC, LMC, and M 31. Including yellow supergiants (YSGs) would move the observed data point slightly upwards in the LMC, where Humphreys et al. (2023) found three YSGs with $\log(L/L_\odot) = 5.7$. No such bright YSGs were found in the SMC (Neugent et al. 2010), M31 (Drout et al. 2009), and our Fig. 2.

The observed metallicity dependence of the cool SG upper luminosity limit, or rather the lack thereof, is visible in Fig. 4. The average luminosity of the third brightest cool SG in the galaxies in our sample has a value of $\log(L/L_\odot) = 5.46$ with a standard deviation of only 0.06.

For comparison, we also consider theoretical cool SG populations based on BoOST models. Similar to what is described in Sect. 4.2, for each galaxy we draw cool SGs until we have as many in the range $5.0 \leq \log(L/L_\odot) \leq 5.4$ as are observed (the only difference is that here each non-rejected model has a statistical weight of 1). Then we identify the third brightest cool SG (orange lines in Fig. 4). We repeat this 20 times for each galaxy, and indicate the probability density of the blue lines with violin plots. The NGC 5253 simulations tend to have brighter cool SGs than the SMC simulations because NGC 5253 contains more dim cool SGs, and the same models are used for these galaxies. Other than that, the model populations show a clear trend, where brighter RSGs are expected to be present in more metal-poor galaxies. Evidently, this is discrepant with our observational results, where bright cool SGs ($\log(L/L_\odot) \gtrsim 5.6$) are absent. We will discuss the astrophysical implications of this at the end of the Discussion section (Sect. 5.4).

5. Discussion

5.1. Sensitivity to warm supergiants in I Zw 18

Above, we found no cool SGs with $\log(L/L_\odot) > 5.6$; $T_{eff} < 7$ kK in I Zw 18. For hotter stars at such luminosities, we are not able to calculate the luminosities as accurately, but they might still show up in the CMD – if they exist. We investigate this further in this section.

In Fig. 5, we show the blue side of the IR CMD of I Zw 18. We also indicate regimes associated with different temperatures and luminosities, based on the MIST BCs. This figure shows that also at bluer colors, the CMD locus associated with $\log(L/L_\odot) \gtrsim$ 5.6 remains empty, at least at $F115W-F200W \gtrsim -0.15$ (temperatures of ∼20 kK and below). The CMD implies the presence of about 25 less luminous warm SGs with $5.0 < \log(L/L_\odot) < 5.6$. In this part of the CMD, the completeness is still expected to be on the order of 50% (Fig. 5; and see Sect. 5.3.2 for further discussions on completeness). We refrain from making quantitative statements for bluer sources (hotter than ∼20 kK) as their inferred luminosity becomes increasingly sensitive to color, while at the same time the errors and completeness progressively get worse with decreasing brightness in the $F200W$ filter. From this analysis, we conclude that the CMD of I Zw 18 indicates that it does not host a sizable population of bright warm SGs ($\log(L/L_\odot) > 5.6$; $7 \leq T_{eff}/\mathrm{kK} \leq 20$).

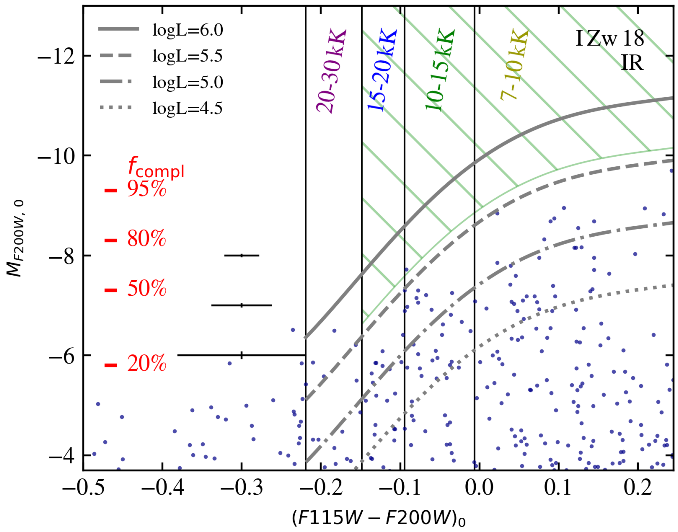

Fig. 5. Similar to the bottom left panel of Fig. 2, but only showing infrared data of I Zw 18, and zoomed in on the bluer side of the CMD. Here we show iso-luminosity lines that extend to bluer colors. The temperature ranges associated with the color intervals bordered by the black vertical lines are written in the plot. The green hatching highlights the empty region associated with $T_{eff} < 20$ kK and $\log(L/L_\odot) > 5.6$. The red ticks indicate the absolute $F200W$ magnitudes at which Bortolini et al. (2024) find a completeness (f_{compl}) of 20%, 50%, 80%, and 95% in the densest region of I Zw 18, R1. With black crosses we show typical observational errors from Bortolini et al. (2024) at absolute $F115W$ magnitudes of -8, -7, and -6, estimated also for R1.

5.2. Comparison with evolutionary models of I Zw 18

In Fig. 6 we show Hertzsprung-Russell diagrams (HRDs) of various evolutionary models with a metallicity similar to I Zw 18's. These include the BoOST models that we used before to synthesize theoretical populations of cool SGs. Additionally, we display PARSEC models (Bressan et al. 2012; Tang et al. 2014, $Z = 0.0005$) and Geneva models (Groh et al. 2019, $Z = 0.0004$, with and without rotation). Finally, we show BPASS single-star models (Eldridge et al. 2017) with both $Z = 0.0001$ and $Z = 0.001$, since neither is particularly close to I Zw 18's metallicity of $Z \approx 0.0004$, and no models with an in-between value have been computed. We refrain from showing MIST models (Dotter 2016; Choi et al. 2016), because most of the models that we downloaded in the mass range 10-150 $M_\odot$ did not evolve through helium burning. For reference, we show the regions of

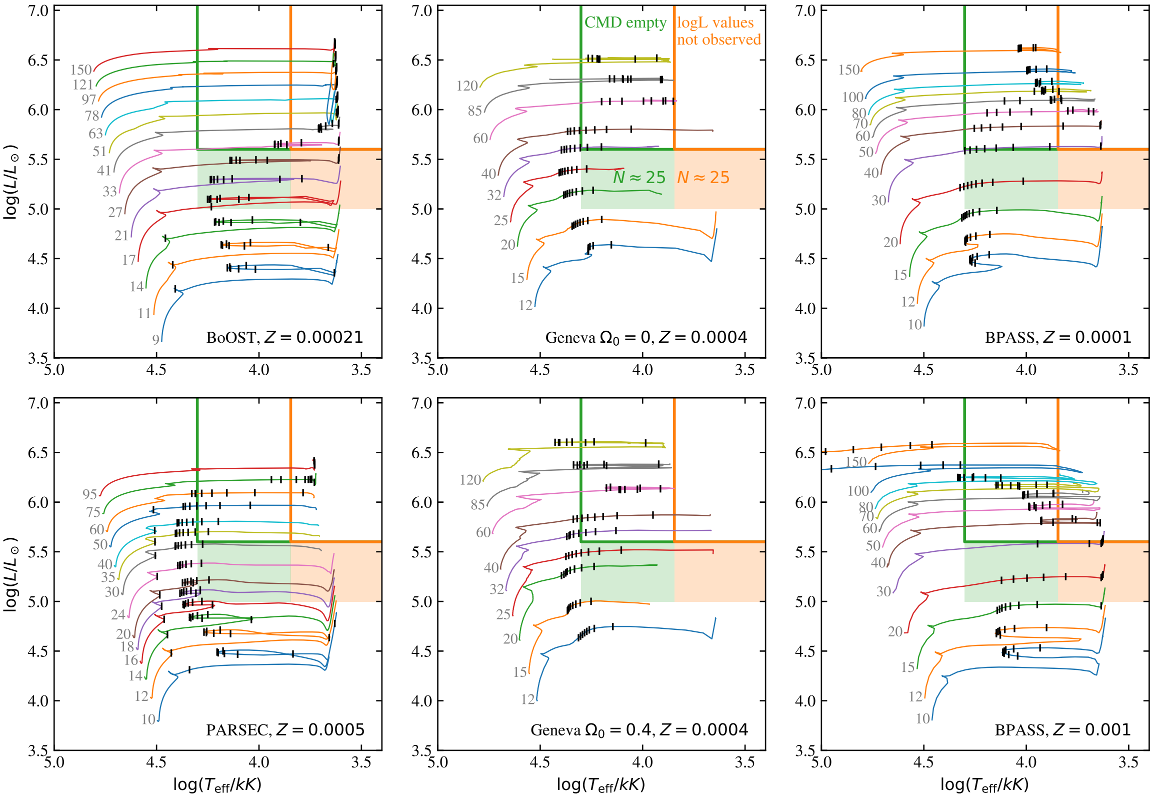

Fig. 6. Hertzsprung-Russell diagrams showing evolutionary tracks with a metallicity similar to I Zw 18. The gray numbers indicate the initial masses of the evolutionary models in Solar units. The black ticks show the position of models at 0.925, 0.935, . . . , 0.995 times the age of the final model of a simulation, to indicate where helium-burning models spend most of their time. The empty region in the CMD of I Zw 18 associated with bright warm sources ($\log(L/L_{\odot}) > 5.6$ and $7 \leq T_{\rm eff}/{\rm kK} < 20$; Fig. 5) is highlighted with an empty green box. The area where we found no bright cool SGs is highlighted with an empty orange box. The areas where we inferred the presence of the order of 25 warm and cool SGs are highlighted with filled green and orange boxes, respectively.

the HRD that seemed unpopulated according to our CMD analysis of warm SGs (Fig. 5) and our cool SG luminosity measurements (Sect. 4.2). We also highlight the HRD regions in which we inferred the presence of ~25 SGs (both warm and cool) in the luminosity range $5.0 < \log(L/L_{\odot}) < 5.6$.

The evolutionary models show differences in the temperatures at which they burn helium, where in particular BoOST models are cooler than the other models during this phase. We attribute this to differences in internal mixing assumptions. Overshooting and (semi-)convection are known to drastically affect post-MS evolution (see e.g., Schootemeijer et al. 2019; Higgins & Vink 2020; Farrell et al. 2022). Also rotational mixing (Maeder & Meynet 2000; Heger et al. 2000) could affect the evolutionary paths. In the range $5.0 < \log(L/L_{\odot}) < 5.4$, PARSEC and Geneva models only predict cool SGs below 7 kK to exist after central helium exhaustion, which lasts less than 0.1% of the stellar lifetime. Given that we inferred the presence of at least 20 cool SGs in that luminosity range, PARSEC and Geneva models would imply that tens of thousands of hydrogen- and helium-burning progenitor stars should exist. This seems unrealistic, given that their combined luminosity would exceed I Zw 18's total luminosity, which is around $10^8\,{\rm L}_{\odot}$[4]. Therefore, Geneva and PARSEC models at I Zw 18 metallicity probably underestimate the cool SG lifetime. In contrast, BoOST models – seemingly correctly – predict longer cool SG lifetimes, but they overpredict the number of bright cool SGs (Sect. 4.2). In the BPASS models with $Z = 0.001$ the blueward evolution is caused by strong RSG mass loss, after which the mass-loss rates become lower, preventing most models to evolve into stars hotter than ~20 kK. At the metallicity of I Zw 18 or lower ($Z \lesssim 0.0004$), none of the sets of evolutionary models shown in Fig. 6 become hot enough to be WR stars. There is, however, observational evidence for WR stars in I Zw 18 (Sect 5.3.4).

In theory, the absence of cool SGs with $\log(L/L_{\odot}) > 5.6$ in I Zw 18 could be a stellar evolution effect that is unrelated to mass loss. That scenario would require the following trend with initial mass: stars with $M_{\rm ini} \lesssim 30\,{\rm M}_{\odot}$ produce the observed cool SGs, while higher-mass stars retain their hydrogen-rich envelopes but evolve into hotter stars with temperatures above 20 kK. However, no set of evolutionary models with I Zw 18 metallicity shows this trend. If anything, they do opposite: brighter helium-burning models tend to be cooler (see the position of the black ticks in Fig. 6). But we note that these models are uncertain, as discussed in the previous paragraph. If they wrongly predict the temperature trend with mass during helium burning, we cannot exclude that $M_{\rm ini} \gtrsim 30\,{\rm M}_{\odot}$ stars in I Zw 18 in reality retain their hydrogen-rich layers, but burn helium at $T_{\rm eff} > 20$ kK.

[4] Obtained using Eq. 1, using $B = 15.98$ from de Vaucouleurs et al. (1991, 1995) and $BC = 0$, which should be appropriate for its color of $B - V \approx 0$ (Papaderos et al. 2002) in an order-of-magnitude estimate.

5.3. Possible caveats

5.3.1. Variability:

Our results could be affected by intrinsic variability of cool SGs. Betelgeuse, for example, is known to display magnitudes in the V-band anywhere in the range $0.2 \lesssim V \lesssim 1.0$ over the last 15 years, and even reached a magnitude of $V \approx 1.7$ during the Great Dimming in 2020 (Jadlovský et al. 2024). Here, we briefly discuss literature results about variability of the brightest cool SG in the Milky Way, M 31, and the Magellanic Clouds.

In the Milky Way, we investigate the five brightest sources of Messineo & Brown (2019) that have epoch photometry[5] in Gaia DR3 (Gaia Collaboration et al. 2023). We find that the standard deviations of the G_{RP} magnitudes of these five sources are between 0.05 and 0.25 (with 0.13 as both average and median). The G_{RP} band has a similar central wavelength as the I band and the $F814W$ band, which are used to construct Fig. 2. In the G_{BP} band (central wavelength similar to the V and $F555W$ bands), the variations were about twice as large as in the G_{RP} band.

Beyond the Milky Way, Yang et al. (2018) found that the brightest RSGs in the LMC have a median absolute deviation of about 0.1 mag in the infrared $WISE1$ band. Soraisam et al. (2018) calculated the root mean square deviation (RMSD) from the mean of the R-band magnitude of RSGs in M 31. Analyzing the five brightest RSGs in their table 1, we find RMSD values in the range of 0.01 mag to 0.37 mag (median: 0.13, average: 0.16). Looking into the five brightest RSGs in the SMC, we find that they have a median dispersion (or variance) in the G_{RP} band of 0.08 mag in the catalog of Maíz Apellániz et al. (2023). For both the M 31 and the SMC case, we get similar results when we include more RSGs.

We conclude that the typical variability of the brightest RSGs in the Magellanic Clouds, M 31, and Milky Way seems to be of the order of 0.1-0.15 mag. This translates into 0.03 - 0.05 dex in $\log(L/L_\odot)$, which is too small to significantly affect our results. Furthermore, in the near-IR RSG variability is significantly smaller than it is at optical wavelengths (see Wang et al. 2025, for further discussion), which adds strength to the luminosities determined with JWST data for the RSG population of I Zw 18.

5.3.2. Crowding and completeness in I Zw 18

At ~18 Mpc, I Zw 18 is the most distant galaxy in our sample, making it prone to crowding issues. This could cause an overestimation of the brightness of individual sources, or it could prevent sources from being detected. Therefore, Bortolini et al. (2024) investigated the errors and completeness of their JWST observations, which are also used for this paper. To do so, they performed artificial star tests (ASTs). In short: these ASTs randomly placed one individual artificial star at a time into the image, the probability of its spatial positioning following the observed surface brightness. Different magnitudes have been explored. For each artificial star the image was reprocessed. It was investigated how often artificial stars of different magnitudes were recovered. This provided magnitude-dependent completeness fractions and errors for a few different regions, from the outskirts of I Zw 18 to the dense central area.

Here, we will consider the completeness fraction in the densest region, called R1 (see Fig. 1 of Bortolini et al. 2024). It contains the vast majority of the cool SGs for which we derived $\log(L/L_\odot) > 5$. R1 is located in the central part of the galaxy's main body and it has an angular size of about 3.5″ (corresponding to ~300 pc at the distance of I Zw 18). For comparison: the angular resolution of JWST is about 0.1″ and the cluster NGC 330 in the SMC would have a projected diameter of ~0.5″ if it were at the distance of I Zw 18.

Bortolini et al. (2024) estimated with their ASTs that in the region R1, for absolute magnitudes of $M_{F200W} < -9$ (corresponding to $\log(L/L_\odot) \gtrsim 5$ for cool SGs) the completeness fraction is 95% or higher (as is also indicated in Fig. 5). Therefore, despite the high concentration of sources in R1, the ASTs suggest that the brightest cool SGs can still be recovered. This result is likely a consequence of how the DOLPHOT software works, namely, by first identifying the brightest sources, thus making it unlikely that they are missed. We note that in the same region, Annibali et al. (2013) find a similar completeness as a function of absolute I magnitude for the data of Aloisi et al. (2007) that are shown in the lower middle panel of Fig. 2. These high estimates for the completeness fraction would imply that our main result – the absence of bright cool SGs – is not strongly affected by completeness issues. As an additional test, we inspect the JWST image to search for potential unresolved clusters. We find one region in R1 with diffuse emission, but in the $F200W$ image its integrated flux is lower than that of the brightest cool SGs in R1. Therefore, it is not possible that this diffuse emission region hosts a cool SG that is brighter than the brightest ones detected. We find no other candidates for unresolved clusters hosting bright cool SGs.

The brightest cool SGs could be clustered together much more than assumed in the ASTs from Bortolini et al. (2024). This could lead us to overestimate their individual luminosities. While it is hard to rule out that this plays a role, it is worth mentioning that in the LMC and M 31, RSGs are more isolated than O stars and WR stars (Smith & Tombleson 2015; Aadland et al. 2018). Also, inspection of the data of Davies et al. (2018) shows that RSGs in the SMC and LMC are spread out rather evenly.

In Sect. 4.2, we noticed that in the range $4.6 < \log(L/L_\odot) < 5$, I Zw 18 contains about five times fewer cool SGs than the theoretical population. This could be explained in part by the dropping completeness fraction of the observed sources. However, since these sources in question have absolute magnitudes of $M_{F200W} \approx -8$ or brighter, where the completeness should still be around 80%, a lower completeness fraction can only partially explain this relatively low number.

5.3.3. Reliability of luminosity measurements in I Zw 18

Hirschauer et al. (2024) found that some of their brightest sources are dusty star candidates, for which they adopt a threshold of $F115W - F444W > 0.5$. Dust can cause self-extinction, which, if severe enough, could cause our method to underestimate stellar luminosities. To investigate if this poses a potential problem, we looked at SMC and LMC data of Davies et al. (2018). In these data, we found no obvious correlation between $J - WISE2$ color (which uses filters with central wavelengths similar to the $F115W$ and $F444W$ filters[6]) and visual extinction A_V, implying that $F444W$ excess does not significantly affect A_V values. Moreover, to derive cool SG luminosities in I Zw 18 we used $F115W$ and $F200W$ magnitudes, which are affected much less by extinction than the V band ($A_{F200W}/A_V \approx 0.08$ according to Wang & Chen 2019). On top of that, I Zw 18 contains only a small amount of dust (Cannon et al. 2002), as is expected for its low metallicity. We conclude that extinction is unlikely to sig-

[5] https://gea.esac.esa.int/archive/

[6] http://svo2.cab.inta-csic.es/theory/fps/

nificantly affect the luminosity measurements based on IR data from JWST.

Furthermore, we note that using JWST data in the IR we found a luminosity of the brightest (and third brightest) cool SG that was similar within 0.02 dex to that obtained from using optical data from Aloisi et al. (2007). This would be unexpected if extinction were to strongly affect our measurements, or if unresolved nearby main-sequence stars were to significantly contribute to the flux. Also, our tests in the SMC (Fig. 1) suggested reasonably high accuracy of our luminosity measurements. Moreover, in the SMC three different methods (IR CMD, optical CMD, and the results from Davies et al. (2018)) yielded a luminosity of the third brightest cool SG within 0.01 dex.

The ASTs by Bortolini et al. (2024) discussed in the previous section suggest that the errors for sources with $M_{F200W} \leq -8$ are of the order of 0.001 mag. This is too low to significantly affect the cool SG luminosities that we derived.

5.3.4. Star-formation history of I Zw 18

The star formation rate (SFR) in I Zw 18 is thought to have varied in time, where relatively many stars formed recently, but some also around 1 Gyr ago or more (Aloisi et al. 2007; Annibali et al. 2013; Bortolini et al. 2024). The recent starburst in I Zw 18 may have been triggered by interaction of its main body with its component C (Kim et al. 2017; McQuinn et al. 2020; Bortolini et al. 2024). It is in principle possible that a recent halt in star formation has caused the absence of the brightest and most short-lived cool SGs, although this explanation would require fine-tuning to achieve the upper luminosity limit of $\log(L/L_\odot) \approx 5.6$ that is also observed in the other galaxies.

In this context, it is of relevance that the presence of WR stars – which are also thought to be luminous helium-burning stars – has been inferred from spectra of I Zw 18. Features of WC (WR stars with strong carbon lines) and WN (WR stars with strong nitrogen lines) stars have been reported, and it was deduced that it hosts some tens of WR stars in total (Izotov et al. 1997; Legrand et al. 1997; de Mello et al. 1998; Brown et al. 2002). The exact number of WR stars in I Zw 18 is probably quite uncertain: first, these numbers are calculated using emission line fluxes per WR star, which are highly uncertain at I Zw 18 metallicity (see also González-Torà et al. 2025); second, these numbers are based on distances around 11 Mpc, which would lead to a ~three times lower number of WR stars than adopting a more recent distance determination of 18 Mpc (Aloisi et al. 2007).

We can speculate that the WR stars in I Zw 18 are more luminous than $\log(L/L_\odot) \approx 5.6$, based on the following arguments. First, in the MW and its direct surroundings, the luminosity of the dimmest WR star increases with decreasing metallicity (Shenar et al. 2020), where $\log(L_{\rm WR,\,min}/L_\odot)$ has a value of 4.9 in the MW, 5.2 in the LMC, and 5.6 in the SMC. Second, a hot stripped star with $\log(L/L_\odot) = 5.1$, which does not manifest itself as a WR star, has been detected in the SMC (Götberg et al. 2023). This further supports the idea that WR stars at low metallicity have to be luminous, in order to drive winds that are dense enough for producing the characteristic WR emission lines. From this it would follow that the absence of cool SGs with $\log(L/L_\odot) \gtrsim 5.6$ in I Zw 18 is not the result of the star formation history, but the result of such luminous helium-burning stars manifesting themselves as different objects such as WR stars.

5.4. Astrophysical implications of the absence of bright cool and warm SGs

Above, we found no cool and warm SGs in low-metallicity galaxies with $\log(L/L_\odot) \gtrsim 5.6$, although we would expect to see them based on theoretical arguments. Also, the stellar evolution models that we analyzed predict that this absence of bright cool and warm SGs is not a stellar evolution effect.

Apart from I Zw 18 (Sect. 5.3.4), WR features have also been reported in the other galaxies that we analyzed and where we found no cool SGs above $\log(L/L_\odot) = 5.6$. NGC 5253 is said to host of the order of 30 to 40 WR stars (Schaerer et al. 1997; Westmoquette et al. 2013). Schild & Testor (1991) and Breysacher et al. (1997) derive a similar number of WR stars for NGC 300. Finally, Brinchmann et al. (2008) report WR features in the spectrum of NGC 4395. In the SMC, LMC, and M 31, many WR stars are observed as individual sources (Crowther 2007).

To summarize: in the galaxies considered in this study, there is, i), an absence of bright cool SGs, ii), a presence of WR stars, and moreover, iii) low-metallicity WR stars are expected to be bright. Together, this implies that low-metallicity massive stars born with $M_{\rm ini} \gtrsim 30\,{\rm M}_\odot$ evolve into hot stars ($T_{\rm eff} > 7$ kK), in many or all cases WR stars. In Sect. 5.4.1 we discuss, from a stellar evolution point of view, what the most likely cause of this is. The implications for stellar populations are discussed in Sect. 5.4.2.

5.4.1. Implications for stellar evolution

Metallicity-independent mass loss. When Humphreys & Davidson (1979) noticed that cool and warm SGs in the LMC and MW had a similar upper luminosity limit, they attributed this to metallicity-independent mass loss. They proposed that late-phase mass loss by luminous blue variable (LBV) stars is at work. This has been supported by Davies et al. (2018), who investigated cool SGs in the SMC and LMC. RSG mass loss could play a similar role (Yang et al. 2023; Zapartas et al. 2025; Antoniadis et al. 2025). Metallicity-independent mass loss seems to be a straightforward explanation for our results in I Zw 18, where we find that the upper luminosity limit for cool SGs is not different than anywhere else. Unfortunately, mass loss rates of evolved stars are hard to pin down (Smith 2014), making it difficult to securely confirm or reject this hypothesis.

Some mechanisms have been proposed for metallicity-independent mass loss (e.g., Kee et al. 2021; Cheng et al. 2024). In this light, it is interesting to mention that the presence of LBV stars has been inferred for very low-metallicity galaxies, even around the metallicity of I Zw 18 (Izotov & Thuan 2009; Pustilnik et al. 2008; Pustilnik & Perepelitsyna 2025).

Internal mixing. It has also been proposed that a combination of metallicity-dependent mass loss and internal mixing processes sets the upper luminosity limit of cool SGs in the Magellanic Clouds and the MW (Higgins & Vink 2020; Sabhahit et al. 2021; Gilkis et al. 2021; Schootemeijer et al. 2019). However, this could lead to metallicity-dependent upper luminosity limits (Higgins & Vink 2020), or a need to fine-tune the mass-loss rates to maintain a metallicity independence (Sabhahit et al. 2021). For the latter, explaining a constant upper luminosity limit of cool SGs over the larger metallicity range shown in Fig. 4 (spanning almost 2 dex, instead of 0.7 dex in their considered range from SMC to MW) might become difficult. Gilkis et al. (2021)

found that models with large overshooting values can explain the observed upper cool SG luminosity limits in the MW, LMC, and SMC. However, they found that especially at SMC metallicity, they predicted too many SGs around $T_{eff} \approx 10$ kK, which lead them to conclude that something was missing in the physics assumptions in models.

Rotational mixing could also play a role, in particular if it is strong enough to induce chemically homogeneous evolution (CHE; e.g., Brott et al. 2011). CHE models remain hot and evolve into hot helium-rich stars (potentially with WR-type spectra) rather than cool SGs. Some of the most hydrogen-poor SMC WR stars could be consistent with CHE (see e.g., Martins et al. 2009; Schootemeijer & Langer 2018; Sharpe et al. 2024; Boco et al. 2025). Therefore, CHE has been invoked to (help) explain the cool SG upper luminosity limit in the SMC (Ramachandran et al. 2019; Boco et al. 2025). We emphasize that to fully explain the observed cool SG luminosity limit, *all* stars above ~30 $M_{\odot}$ must undergo CHE. However, in the SMC, the properties of these stars in HRDs (Blaha & Humphreys 1989; Massey et al. 1995; Schootemeijer et al. 2021; Bestenlehner et al. 2025) are the opposite of what a population CHE models would predict. The area near the zero-age main sequence in those HRDs, where CHE models spend around 90% of their lifetime, is almost completely void. And at cooler temperatures, at which CHE models spend little to no time, several tens of stars are observed above the 30 $M_{\odot}$ track. Another challenge to this CHE scenario is that 90% of massive SMC stars appear to rotate too slowly to undergo CHE (Boco et al. 2025). Furthermore, CHE models struggle to simultaneously explain the observed projected rotation velocity, temperature, and surface abundances of most SMC WR stars (Hainich et al. 2015; Vink & Harries 2017; Schootemeijer & Langer 2018; Martins 2023).

Binary interaction. Most massive stars are observed in binaries (Sana et al. 2012, 2025). The luminosity distribution of cool SGs would be affected by binary interaction if it prevents stars from evolving into cool SGs. However, a high binary fraction among all massive stars would then result in a systematic shift of the cool SG luminosity distribution instead of the observed drop at $\log(L/L_{\odot}) \approx 5.6$. To explain this drop we see two possibilities. First, the binary fraction could change with initial mass, where above 30 $M_{\odot}$ it approaches unity but at lower masses it does not. The second explanation would be that the binary fraction is near unity for all massive stars, but that the outcome of binary interaction would be different above 30 $M_{\odot}$ (never cool SGs) and below 30 $M_{\odot}$ (cool SG production possible).

If any of the two explanations work in practice remains to be seen. Regarding the first explanation, in the BLOeM sample of massive SMC stars (Shenar et al. 2024), the binary fraction appears to be constant rather than increase above 30 $M_{\odot}$ (Britavskiy et al. 2025; Sana et al. 2025; Villaseñor et al. 2025; Bestenlehner et al. 2025, Fig. E1 of the latter). These results are based on nine out of 25 epochs of the survey; we expect a more definitive result upon its completion. For the second explanation, at first glance models of accretor stars (Schneider et al. 2024) and mergers (Menon et al. 2024) do not appear to show a sharp transition in cool SG lifetimes around 30 $M_{\odot}$. It is also worth mentioning that, if binary stripping were the only method that is operational to strip the outer layers of evolved massive stars, it seems hard to explain that 50-60% of WR stars appear to be genuinely single in both the MW (Deshmukh et al. 2024) and the SMC (Foellmi et al. 2003; Schootemeijer et al. 2024, see sect. 7.1 of the latter for a detailed discussion). Despite these potential challenges, major uncertainties exist in the prevalence of distant and low-mass binary companions, and in the physics of the mass accretion and merger processes. This argues against drawing strong conclusions on the impact of binaries on the observed upper luminosity limit of cool SGs.

Interpretation. We argue that metallicity-independent mass loss is the most straightforward explanation for a metallicity-independent cool SG luminosity limit (Fig. 4). To solidify this assessment or to disprove it, we encourage future studies on, for example, binary population synthesis, mass loss rates of evolved massive stars at low metallicity, or more bias-corrected measurements of binary fractions of metal-poor WR stars and their hydrogen-burning progenitor stars.

FRANEC (Limongi & Chieffi 2018) and MIST (Dotter 2016; Choi et al. 2016) models adopt late-phase mass loss of massive stars that is independent of metallicity. If our interpretation is correct, this assumption is favored over the metallicity-dependence of late-phase mass loss in the PARSEC (Bressan et al. 2012; Tang et al. 2014), Geneva (Georgy et al. 2013; Groh et al. 2019), and Bonn models (Brott et al. 2011; Schootemeijer et al. 2019; Szécsi et al. 2022). Some works assume that hydrogen-rich layers of stars with initial masses above above 30 $M_{\odot}$ would end up in their BH remnants (Fryer et al. 2012). If their hydrogen-rich layers are shed instead even at low metallicity, this would also set a limitation on the final stellar masses before core collapse, and, therefore, on BH remnant masses (see, e.g., Schootemeijer et al. 2024, their fig. 10).

5.4.2. Implications for He^{+}-ionizing emission from stellar populations

For stellar populations, the important question is *if* massive stars evolve into hot helium-rich stars; not so much if, for example, binary or wind stripping is at work. Below we discuss potential consequences for ionizing radiation and chemical evolution in galaxies for a scenario in which low-metallicity stars born more massive than ~30 $M_{\odot}$ evolve into hot helium-rich stars.

Previous work (Szécsi et al. 2015, 2025; Kubátová et al. 2019) has already proposed that massive stars with I Zw 18 metallicity could become hot enough to produce hard ionizing radiation, while their low metallicity prevents them from launching dense winds. In their scenario, massive stars undergoing extremely rapid rotation experience chemically homogeneous evolution (CHE) induced by efficient rotational mixing. Here, we propose a scenario that is similar, but in which wind-stripping rather than CHE creates the hot stars with weak winds that allow hard ionizing radiation to escape the stellar wind, and that thus can produce emission of for example He II and C IV.

We illustrate this scenario in Fig. 7. The figure shows where we expect single stars to produce hard ionizing radiation, as a function of metallicity and luminosity. Since our findings and those in the literature imply that cool SGs (which are too cool to produce hard ionizing photons) exist up to a metallicity-independent upper luminosity limit, we cross out the area with $\log(L/L_{\odot}) < 5.6$. Furthermore, Sander & Vink (2020) predict that the onset of optically thick WR winds can dramatically reduce the He^{+}-ionizing flux (by a factor of 10^{10}; their fig. 22). We thus also cross out the part in Fig. 7 where WR winds are expected for hot helium-rich stars. Observations show that the onset of the WR phenomenon is metallicity dependent (Hainich et al. 2014, 2015; Hamann et al. 2019; Shenar et al. 2020). We adopt the minimum WR luminosity from Shenar et al. (2020)

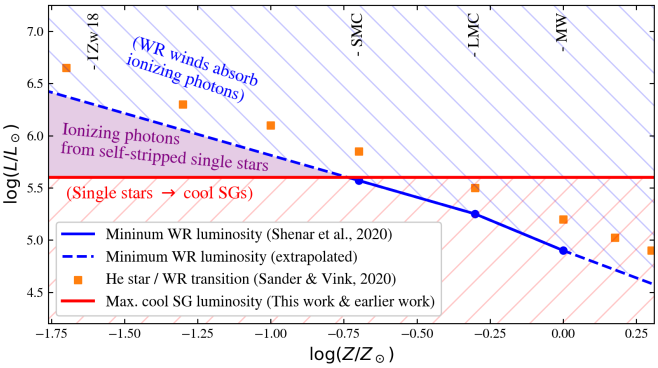

Fig. 7. Diagram illustrating the window of opportunity for the production of hard ionizing radiation in our single-star wind-stripping scenario (highlighted with purple shading). The blue and red hatched regions indicate where dense WR winds and evolution into cool SGs would prevent the production of hard ionizing radiation, respectively. The values for minimum WR luminosity (blue line) are taken from Shenar et al. (2020) and the He star / WR transition in orange are the points where Sander & Vink (2020) predict the onset of multiple scattering ($\eta = 1$), below which, winds are expected to be weak.

and extrapolate outside of their considered metallicity range. It is reassuring that, apart from a slight offset, the result of this extrapolation is similar to the helium star / WR boundary in wind models from Sander & Vink (2020). This metallicity dependence of the onset of WR winds would introduce a window of opportunity for the production of hard ionizing radiation at sub-SMC metallicity, which we mark with purple shading in Fig. 7.

Our scenario has a few caveats. First, in some cases, WR stars might emit more He^+-ionizing photons than the models of Sander & Vink (2020) suggest (Sander et al. 2025; González-Torà et al. 2025; Sixtos et al. 2023). Second, our scenario relies on helium-burning massive stars in I Zw 18 with $\log(L/L_\odot) > 5.6$ to evolve into hot helium-rich stars, whereas we have only shown that they are absent up to ~20 kK. It could be that some helium-burning stars of $M_{ini} \gtrsim 30\,M_\odot$ evolve into intermediate-temperature objects instead (such cases have been reported in binary systems; one by Pauli et al. (2022b), and four dimmer counterparts at $\log(L/L_\odot) < 5.0$ by Ramachandran et al. (2023, 2024). Also, since about 70% of massive stars are thought to be in binaries (Sana et al. 2012, 2025), binary stripping could produce the majority of hot and luminous helium-rich stars above $\log(L/L_\odot) = 5.6$ while also contributing at lower luminosities (Götberg et al. 2018; Hovis-Afflerbach et al. 2025).

On the other hand, the number of binary-stripped stars at low metallicity might be relatively small if low-Z stars tend to stay compact until late helium burning (Hovis-Afflerbach et al. 2025). Also, Sana et al. (2012) estimated that only 30% of massive stars undergo binary stripping, and Schürmann & Langer (2024) found that binaries might be even more likely to merge upon interacting than previously thought. Therefore, it is plausible that wind stripping is more important than binary stripping to produce luminous helium-rich stars at low metallicity. This is corroborated by the case of the SMC, which hosts five binary WR stars and seven single ones (Foellmi et al. 2003; Schootemeijer et al. 2024). Moreover, an advantage of the wind-stripping scenario is that it does not rely on CHE, which has not been proven to occur in nature (Sect. 5.4.1).

Popular spectral synthesis tools for stellar populations rely on evolutionary models discussed in Sect 5.2 (BPASS (Eldridge et al. 2017), and Geneva models in case of Starburst99; Leitherer et al. 1999, 2014). As such, these codes are built on single star tracks that appear to not well represent massive stellar evolution at I Zw 18 metallicity, and in fact entirely overestimate the number of cool and/or warm SGs. While BPASS can account for binary interaction, it does not include the sharp decrease in wind mass loss below the single-scattering limit $\eta = 1$ that Sander & Vink (2020) predict. BPASS can even predict lower ionizing photon emission rates at low metallicity than Starburst99 (see below). If all low-metallicity stars with $M_{ini} \gtrsim 30\,M_\odot$ can instead evolve into hot stars with weak winds, it means that their predicted emission rates of hard ionizing photons from spectral synthesis codes could be significantly underestimated. We will investigate this below for the case of I Zw 18.

By measuring the integrated narrow-line He II emission of I Zw 18, Kehrig et al. (2015) estimated that its ensemble of ionizing sources emits He^+-ionizing photons at a rate of $Q(He^+) = 1.3 \cdot 10^{50}\,s^{-1}$. They concluded that an unrealistically large population of WR stars (more than 400) is required to explain this number. For a weak-wind helium star around $\log(L/L_\odot) = 6$, a value close to $Q(He^+) = 10^{49}\,s^{-1}$ is expected (Sander & Vink 2020). Explaining the inferred He^+-ionization emission rate in I Zw 18 would require only about 20 of such stars, which appears to be consistent with our findings in Sects. 4.2 and 5.1.

We compare with the predicted He^+-ionizing emission rate of I Zw 18 from spectral population synthesis codes. Adopting the recent star-formation rate of 0.6 $M_\odot$/yr from Bortolini et al. (2024), Starburst99 predicts $Q(He^+) \approx 2.5 \cdot 10^{50}\,s^{-1}$ (Leitherer et al. 1999, their fig. 82e), while BPASS predicts $Q(He^+) \approx 1.5 \cdot 10^{50}\,s^{-1}$ (Stanway et al. 2016, their fig 11). For both predictions, we used the lowest metallicity underlying models ($Z = 0.001$) and note that this lowest metallicity is higher by about a factor of 3 than the metallicity of I Zw 18. In Starburst99, the He^+-ionizing photons are produced by wind-stripped WR stars born with 85 $M_\odot$ or more (models from Meynet et al. 1994), while in BPASS, they mostly come from binary-stripped stars and accretor stars undergoing CHE following spin-up triggered by binary mass transfer (Eldridge et al. 2011; Stanway et al. 2016).

This good agreement between the He^+-ionizing emission rates from observations in I Zw 18 and the theoretical predictions of BPASS and Starburst99 does not signal a need for extra emission by weak-wind self-stripped stars (purple shading in Fig. 7). However, those theoretical values are proportional to the SFR, which, in the case of Bortolini et al. (2024), is based on PARSEC models. As we have seen in Sect. 5.4.1, these models are likely to strongly underestimate cool SG lifetimes at I Zw 18 metallicity, which would lead to an overestimated SFR. In Appendix A we find a minimum SFR for I Zw 18 of 0.019 $M_\odot$/yr based on the assumption that the 28 observed cool SGs at $5.0 < \log(L/L_\odot) < 5.6$ are in a helium-burning phase that lasts 7% of their lifetime. If the true SFR of I Zw 18 were closer to this value, BPASS and Starburst99 could underpredict $Q(He^+)$ by about a factor ten, and extra sources of this emission would indeed be required. Future short-wavelength observations of massive main-sequence stars in I Zw 18 may provide a less model-dependent value of its SFR. This would give vital clues for our self-stripping scenario as well as Starburst99 and BPASS models.

5.4.3. Implications for nitrogen abundances in high-redshift galaxies

Puzzlingly high nitrogen abundances and [N/O] ratios have been observed in high-redshift low-metallicity galaxies (e.g., Bunker et al. 2023; Cameron et al. 2023; Arellano-Córdova et al. 2025). Vink (2023) argues that CNO-processed winds of very massive stars ($M > 100\,M_\odot$) are a compelling explanation for these high nitrogen abundances. According to Vink (2023), alternative explanations have different drawbacks: asymptotic giant branch (Timmes et al. 1995) stars would not explain the observed Na-N anti-correlation, supermassive stars ($M > 1000\,M_\odot$ Nandal et al. 2024a) and stars undergoing rotationally-induced CHE (Roy et al. 2021; Nandal et al. 2024b, see also Sect. 5.4.1) have never been directly observed, and stars with $M < 100\,M_\odot$ would have too weak winds. If the absence of bright cool SGs above $\sim 30\,M_\odot$ at low metallicity is indeed caused by the loss of their hydrogen-rich layers, including those that are CNO-processed, then stars above this mass limit could also contribute to the observed nitrogen enrichment in high-redshift galaxies.

6. Conclusions

In this study, we used archival HST and JWST photometry data of four dwarf galaxies to derive the luminosity distributions of their cool SG (T_{eff}/kK < 7) populations. We combined this sample with cool SGs in the SMC, LMC, and M 31 with known luminosities. The resulting ensemble of studied galaxies covers a metallicity range of $1/40 \lesssim Z/Z_\odot \lesssim 1.5$. The same picture emerges at all metallicities, both in this work and in literature studies: cool SGs with $\log(L/L_\odot) > 5.6$ are absent, while many cool SGs are observed at lower luminosities. By including I Zw 18, our work pushes the boundary from $Z_\odot/5$ to $Z_\odot/40$.

We found that theoretical stellar populations predict that helium-burning stars with $\log(L/L_\odot) > 5.6$ should be present. In I Zw 18 ($Z/Z_\odot \approx 1/40$), we investigated whether the explanation for the absence of cool SGs at these luminosities could be that the most massive stars evolve into warm SGs ($7 < T_{eff}/\mathrm{kK} < 20$). This does not seem to be the case, because the locus in the CMD where such stars are expected to show up is empty. This implies that in I Zw 18, stars that are born more massive than $\sim 30\,M_\odot$ evolve into neither cool SGs nor warm SGs.

In the literature, the presence of a multitude of WR stars has been spectroscopically inferred for all galaxies that we investigated, including I Zw 18. Combining this with our findings on the absence of bright cool and warm SGs and previous studies in M 31, the MW, and the Magellanic Clouds, a convergent picture seems to emerge in which, even at extremely low metallicity, stars above $\sim 30\,M_\odot$ evolve into hot stars instead. How hot and helium-rich these stars tend to be, and how often they display WR features, remains to be determined. But it seems likely that they tend to lose most of their hydrogen-rich outer layers, since all considered evolutionary models above $30\,M_\odot$ that retain those layers manifest themselves as cool or warm SGs.

From a stellar-evolution point of view, we argue that the most straightforward explanation for the metallicity-independent cool SG upper luminosity limit is metallicity-independent mass loss during the LBV or cool SG phase. This would limit the masses of BH descendants from (extremely) low-metallicity massive stars. Also, our results indicate that low-metallicity massive stars born with $30 \lesssim M_{ini}/M_\odot \lesssim 100$ could contribute to explaining the observed high nitrogen abundances in high-redshift galaxies.

As a possible pathway to produce hard ionizing radiation at low metallicity, we propose a scenario in which single stars undergo self-stripping. There, independent of metallicity, evolved stars above the observed cool SG luminosity limit of $\log(L/L_\odot) \approx 5.6$ shed their hydrogen-rich layers and become hot objects. Since the minimum luminosity for the WR phenomenon to arise increases with decreasing metallicity, below SMC metallicity a window of opportunity opens for hot helium-rich stars in which their hard ionizing photons avoid being absorbed in a dense WR wind. This could help to explain the signatures of hard ionizing photons observed in low-metallicity galaxies, for example through emission of He II and C IV.

References

Aadland, E., Massey, P., Neugent, K. F., & Drout, M. R. 2018, AJ, 156, 294
Abbott, B. P., Abbott, R., Abbott, T. D., et al. 2016, Physical Review Letters, 116, 061102
Abril-Melgarejo, V., James, B. L., Aloisi, A., et al. 2024, ApJ, 973, 173
Aloisi, A., Clementini, G., Tosi, M., et al. 2007, ApJ, 667, L151
Annibali, F., Cignoni, M., Tosi, M., et al. 2013, AJ, 146, 144
Antoniadis, K., Zapartas, E., Bonanos, A. Z., et al. 2025, arXiv e-prints, arXiv:2503.05876
Arellano-Córdova, K. Z., Berg, D. A., Mingozzi, M., et al. 2025, arXiv e-prints, arXiv:2507.11658
Backs, F., Brands, S. A., de Koter, A., et al. 2024, A&A, 692, A88
Bergemann, M., Hoppe, R., Semenova, E., et al. 2021, MNRAS, 508, 2236
Bestenlehner, J. M., Crowther, P. A., Bronner, V. A., et al. 2025, MNRAS, 540, 3523
Blaha, C. & Humphreys, R. M. 1989, AJ, 98, 1598
Boco, L., Mapelli, M., Sander, A. A. C., et al. 2025, arXiv e-prints, arXiv:2507.00137
Bonanos, A. Z. 2025, Galaxies, 13, 66
Bortolini, G., Östlin, G., Habel, N., et al. 2024, A&A, 689, A146
Bressan, A., Marigo, P., Girardi, L., et al. 2012, MNRAS, 427, 127
Breysacher, J., Azzopardi, M., Testor, G., & Muratorio, G. 1997, A&A, 326, 976
Brinchmann, J., Kunth, D., & Durret, F. 2008, A&A, 485, 657
Britavskiy, N., Mahy, L., Lennon, D. J., et al. 2025, A&A, 698, A40
Brott, I., de Mink, S. E., Cantiello, M., et al. 2011, A&A, 530, A115
Brown, T. M., Heap, S. R., Hubeny, I., Lanz, T., & Lindler, D. 2002, ApJ, 579, L75
Bunker, A. J., Saxena, A., Cameron, A. J., et al. 2023, A&A, 677, A88
Cameron, A. J., Katz, H., Rey, M. P., & Saxena, A. 2023, MNRAS, 523, 3516
Cameron, A. J., Katz, H., Witten, C., et al. 2024, MNRAS, 534, 523
Cannon, J. M., Skillman, E. D., Garnett, D. R., & Dufour, R. J. 2002, ApJ, 565, 931
Cedrés, B. & Cepa, J. 2002, A&A, 391, 809
Cheng, S. J., Goldberg, J. A., Cantiello, M., et al. 2024, ApJ, 974, 270
Choi, J., Dotter, A., Conroy, C., et al. 2016, ApJ, 823, 102
Choudhury, S., de Grijs, R., Bekki, K., et al. 2021, MNRAS, 507, 4752
Cioni, M. R. L., Girardi, L., Marigo, P., & Habing, H. J. 2006, A&A, 452, 195
Conti, P. S. & Vacca, W. D. 1994, ApJ, 423, L97
Costa, G., Bressan, A., Mapelli, M., et al. 2021, MNRAS, 501, 4514
Crowther, P. A. 2007, ARA&A, 45, 177
Dalcanton, J. J., Williams, B. F., Seth, A. C., et al. 2009, ApJS, 183, 67
Davidge, T. J. 2007, AJ, 134, 1799
Davies, B., Crowther, P. A., & Beasor, E. R. 2018, MNRAS, 478, 3138
Davies, B., Kudritzki, R.-P., Gazak, Z., et al. 2015, ApJ, 806, 21
de Mello, D. F., Schaerer, D., Heldmann, J., & Leitherer, C. 1998, ApJ, 507, 199
de Vaucouleurs, G., de Vaucouleurs, A., Corwin, H. G., et al. 1995, VizieR Online Data Catalog: Third Reference Cat. of Bright Galaxies (RC3) (de Vaucouleurs+ 1991), VizieR On-line Data Catalog: VII/155. Originally published in: Springer-Verlag: New York, (1991)
de Vaucouleurs, G., de Vaucouleurs, A., Corwin, Jr., H. G., et al. 1991, Third Reference Catalogue of Bright Galaxies
de Wit, S., Bonanos, A. Z., Antoniadis, K., et al. 2024, A&A, 689, A46
Deshmukh, K., Sana, H., Mérand, A., et al. 2024, A&A, 692, A109
Dolphin, A. E. 2000, PASP, 112, 1383
Dotter, A. 2016, ApJS, 222, 8
Drout, M. R., Massey, P., Meynet, G., Tokarz, S., & Caldwell, N. 2009, ApJ, 703, 441
Eldridge, J. J., Langer, N., & Tout, C. A. 2011, MNRAS, 414, 3501
Eldridge, J. J., Stanway, E. R., Xiao, L., et al. 2017, PASA, 34, e058
Farrell, E., Groh, J. H., Meynet, G., & Eldridge, J. J. 2022, MNRAS, 512, 4116
Foellmi, C., Moffat, A. F. J., & Guerrero, M. A. 2003, MNRAS, 338, 360
Fryer, C. L., Belczynski, K., Wiktorowicz, G., et al. 2012, ApJ, 749, 91
Gaia Collaboration, Vallenari, A., Brown, A. G. A., et al. 2023, A&A, 674, A1

Gazak, J. Z., Kudritzki, R., Evans, C., et al. 2015, ApJ, 805, 182
Georgy, C., Ekström, S., Eggenberger, P., et al. 2013, A&A, 558, A103
Gilkis, A., Shenar, T., Ramachandran, V., et al. 2021, MNRAS, 503, 1884
González-Torà, G., Sander, A. A. C., Egorova, E., et al. 2025, arXiv e-prints, arXiv:2509.04569
Gordon, K. D., Clayton, G. C., Misselt, K. A., Landolt, A. U., & Wolff, M. J. 2003, ApJ, 594, 279
Götberg, Y., de Mink, S. E., Groh, J. H., et al. 2018, A&A, 615, A78
Götberg, Y., Drout, M. R., Ji, A. P., et al. 2023, ApJ, 959, 125
Graczyk, D., Pietrzyński, G., Thompson, I. B., et al. 2020, ApJ, 904, 13
Groh, J. H., Ekström, S., Georgy, C., et al. 2019, A&A, 627, A24
Hainich, R., Pasemann, D., Todt, H., et al. 2015, A&A, 581, A21
Hainich, R., Rühling, U., Todt, H., et al. 2014, A&A, 565, A27
Hamann, W. R., Gräfener, G., Liermann, A., et al. 2019, A&A, 625, A57
Harris, J. & Zaritsky, D. 2004, AJ, 127, 1531
Harris, J. & Zaritsky, D. 2009, AJ, 138, 1243
Hayes, M. J., Saldana-Lopez, A., Citro, A., et al. 2025, ApJ, 982, 14
Heger, A., Langer, N., & Woosley, S. E. 2000, ApJ, 528, 368
Helou, G., Roussel, H., Appleton, P., et al. 2004, ApJS, 154, 253
Higgins, E. R. & Vink, J. S. 2020, A&A, 635, A175
Hirschauer, A. S., Crouzet, N., Habel, N., et al. 2024, AJ, 168, 23
Hovis-Afflerbach, B., Götberg, Y., Schootemeijer, A., et al. 2025, A&A, 697, A239
Humphreys, R. M. & Davidson, K. 1979, ApJ, 232, 409
Humphreys, R. M. & Davidson, K. 1994, PASP, 106, 1025
Humphreys, R. M., Jones, T. J., & Martin, J. C. 2023, AJ, 166, 50
Izotov, Y. I., Foltz, C. B., Green, R. F., Guseva, N. G., & Thuan, T. X. 1997, ApJ, 487, L37
Izotov, Y. I. & Thuan, T. X. 2009, ApJ, 690, 1797
Izotov, Y. I. & Thuan, T. X. 2016, MNRAS, 457, 64
Jadlovský, D., Granzer, T., Weber, M., et al. 2024, A&A, 685, A124
Kang, X., Kudritzki, R.-P., Gong, X., & Zhang, F. 2025, A&A, 701, A2
Kee, N. D., Sundqvist, J. O., Decin, L., de Koter, A., & Sana, H. 2021, A&A, 646, A180
Kehrig, C., Vílchez, J. M., Pérez-Montero, E., et al. 2015, ApJ, 801, L28
Kim, J., Chung, A., Wong, O. I., et al. 2017, A&A, 605, A54
Kroupa, P. 2001, MNRAS, 322, 231
Kubátová, B., Szécsi, D., Sander, A. A. C., et al. 2019, A&A, 623, A8
Lalleman, M., Turbang, K., Callister, T., & van Remortel, N. 2025, A&A, 698, A85
Lamers, H. J. G. L. M. & Fitzpatrick, E. L. 1988, ApJ, 324, 279
Lebouteiller, V., Heap, S., Hubeny, I., & Kunth, D. 2013, A&A, 553, A16
Legrand, F., Kunth, D., Roy, J. R., Mas-Hesse, J. M., & Walsh, J. R. 1997, A&A, 326, L17
Leitherer, C., Ekström, S., Meynet, G., et al. 2014, ApJS, 212, 14
Leitherer, C., Schaerer, D., Goldader, J. D., et al. 1999, ApJS, 123, 3
Levesque, E. M., Massey, P., Plez, B., & Olsen, K. A. G. 2009, AJ, 137, 4744
Lewis, A. R., Dolphin, A. E., Dalcanton, J. J., et al. 2015, ApJ, 805, 183
Li, S., Riess, A. G., Busch, M. P., et al. 2021, ApJ, 920, 84
Limongi, M. & Chieffi, A. 2018, ApJS, 237, 13
López-Sánchez, Á. R., Koribalski, B. S., van Eymeren, J., et al. 2012, MNRAS, 419, 1051
Lovegrove, E. & Woosley, S. E. 2013, ApJ, 769, 109
Maeder, A. & Meynet, G. 2000, A&A, 361, 159
Maíz Apellániz, J., Holgado, G., Pantaleoni González, M., & Caballero, J. A. 2023, A&A, 677, A137
Martins, F. 2023, A&A, 680, A22
Martins, F., Hillier, D. J., Bouret, J. C., et al. 2009, A&A, 495, 257
Massey, P., Lang, C. C., Degioia-Eastwood, K., & Garmany, C. D. 1995, ApJ, 438, 188
McDonald, S. L. E., Davies, B., & Beasor, E. R. 2022, MNRAS, 510, 3132
McQuinn, K. B. W., Berg, D. A., Skillman, E. D., et al. 2020, ApJ, 891, 181
Menon, A., Ercolino, A., Urbaneja, M. A., et al. 2024, ApJ, 963, L42
Messineo, M. & Brown, A. G. A. 2019, AJ, 158, 20
Meynet, G., Maeder, A., Schaller, G., Schaerer, D., & Charbonnel, C. 1994, A&AS, 103, 97
Micheva, G., Roth, M. M., Weilbacher, P. M., et al. 2022, A&A, 668, A74
Mingozzi, M., James, B. L., Arellano-Córdova, K. Z., et al. 2022, ApJ, 939, 110
Mingozzi, M., James, B. L., Berg, D. A., et al. 2024, ApJ, 962, 95
Mokiem, M. R., de Koter, A., Vink, J. S., et al. 2007, A&A, 473, 603
Monreal-Ibero, A., Walsh, J. R., & Vílchez, J. M. 2012, A&A, 544, A60
Munoz-Sanchez, G., Kalitsounaki, M., de Wit, S., et al. 2024, arXiv e-prints, arXiv:2411.19329
Nally, C., Jones, O. C., Lenkić, L., et al. 2024, MNRAS, 531, 183
Nandal, D., Regan, J. A., Woods, T. E., et al. 2024a, A&A, 683, A156
Nandal, D., Sibony, Y., & Tsiatsiou, S. 2024b, A&A, 688, A142
Nandi, P., Stalin, C. S., Saikia, D. J., et al. 2023, ApJ, 950, 81
Neugent, K. F. & Massey, P. 2023, AJ, 166, 68
Neugent, K. F., Massey, P., Skiff, B., et al. 2010, ApJ, 719, 1784
Ohnaka, K., Hofmann, K. H., Weigelt, G., et al. 2024, A&A, 691, L15
Olivier, G. M., Berg, D. A., Chisholm, J., et al. 2022, ApJ, 938, 16
Paczyński, B. 1967, Acta Astron., 17, 355
Papaderos, P., Izotov, Y. I., Thuan, T. X., et al. 2002, A&A, 393, 461
Patrick, L. R., Evans, C. J., Davies, B., et al. 2016, MNRAS, 458, 3968
Pauli, D., Langer, N., Aguilera-Dena, D. R., Wang, C., & Marchant, P. 2022a, A&A, 667, A58
Pauli, D., Oskinova, L. M., Hamann, W. R., et al. 2022b, A&A, 659, A9
Pietrzyński, G., Graczyk, D., Gallenne, A., et al. 2019, Nature, 567, 200
Pustilnik, S. A. & Perepelitsyna, Y. A. 2025, A&A, 695, L7
Pustilnik, S. A., Tepliakova, A. L., Kniazev, A. Y., & Burenkov, A. N. 2008, MNRAS, 388, L24
Ramachandran, V., Hamann, W. R., Oskinova, L. M., et al. 2019, A&A, 625, A104
Ramachandran, V., Klencki, J., Sander, A. A. C., et al. 2023, A&A, 674, L12
Ramachandran, V., Sander, A. A. C., Pauli, D., et al. 2024, A&A, 692, A90
Rate, G. & Crowther, P. A. 2020, MNRAS, 493, 1512
Rizzi, L., Bresolin, F., Kudritzki, R.-P., Gieren, W., & Pietrzyński, G. 2006, ApJ, 638, 766
Roy, A., Dopita, M. A., Krumholz, M. R., et al. 2021, MNRAS, 502, 4359
Sabbi, E., Calzetti, D., Ubeda, L., et al. 2018, ApJS, 235, 23
Sabhahit, G. N., Vink, J. S., Higgins, E. R., & Sander, A. A. C. 2021, MNRAS, 506, 4473
Salpeter, E. E. 1955, ApJ, 121, 161
Sana, H., de Mink, S. E., de Koter, A., et al. 2012, Science, 337, 444
Sana, H., Shenar, T., Bodensteiner, J., et al. 2025, arXiv e-prints, arXiv:2509.12488
Sander, A., Todt, H., Hainich, R., & Hamann, W. R. 2014, A&A, 563, A89
Sander, A. A. C., Lefever, R. R., Josiek, J., et al. 2025, arXiv e-prints, arXiv:2508.18410
Sander, A. A. C. & Vink, J. S. 2020, MNRAS, 499, 873
Saxena, A., Pentericci, L., Mirabelli, M., et al. 2020, A&A, 636, A47
Schaerer, D., Contini, T., Kunth, D., & Meynet, G. 1997, ApJ, 481, L75
Schild, H. & Testor, G. 1991, A&A, 243, 115
Schneider, F. R. N., Podsiadlowski, P., & Laplace, E. 2024, A&A, 686, A45
Schootemeijer, A. & Langer, N. 2018, A&A, 611, A75
Schootemeijer, A., Langer, N., Grin, N. J., & Wang, C. 2019, A&A, 625, A132
Schootemeijer, A., Langer, N., Lennon, D., et al. 2021, A&A, 646, A106
Schootemeijer, A., Shenar, T., Langer, N., et al. 2024, A&A, 689, A157
Schürmann, C. & Langer, N. 2024, A&A, 691, A174
Senchyna, P., Stark, D. P., Chevallard, J., et al. 2019, MNRAS, 488, 3492
Sharpe, K., van Son, L. A. C., de Mink, S. E., et al. 2024, ApJ, 966, 9
Shenar, T., Bodensteiner, J., Sana, H., et al. 2024, A&A, 690, A289
Shenar, T., Gilkis, A., Vink, J. S., Sana, H., & Sander, A. A. C. 2020, A&A, 634, A79
Shenar, T., Hainich, R., Todt, H., et al. 2016, A&A, 591, A22
Shenar, T., Sablowski, D. P., Hainich, R., et al. 2019, A&A, 627, A151
Sixtos, A., Wofford, A., Sander, A. A. C., & Peimbert, A. 2023, MNRAS, 519, 5656
Skillman, E. D. & Kennicutt, Robert C., J. 1993, ApJ, 411, 655
Skrutskie, M. F., Cutri, R. M., Stiening, R., et al. 2006, AJ, 131, 1163
Smirnova, K. I., Wiebe, D. S., Moiseev, A. V., & Jozsa, G. I. G. 2020, Astrophysical Bulletin, 75, 234
Smith, N. 2014, ARA&A, 52, 487
Smith, N. & Tombleson, R. 2015, MNRAS, 447, 598
Soraisam, M. D., Bildsten, L., Drout, M. R., et al. 2018, ApJ, 859, 73
Stanway, E. R., Eldridge, J. J., & Becker, G. D. 2016, MNRAS, 456, 485
Stark, D. P., Richard, J., Charlot, S., et al. 2015, MNRAS, 450, 1846
Szécsi, D., Agrawal, P., Wünsch, R., & Langer, N. 2022, A&A, 658, A125
Szécsi, D., Langer, N., Yoon, S.-C., et al. 2015, A&A, 581, A15
Szécsi, D., Tramper, F., Kubátová, B., et al. 2025, arXiv e-prints, arXiv:2506.21442
Tang, J., Bressan, A., Rosenfield, P., et al. 2014, MNRAS, 445, 4287
TensorFlow Developers. 2022, TensorFlow
Thim, F., Hoessel, J. G., Saha, A., et al. 2004, AJ, 127, 2322
Timmes, F. X., Woosley, S. E., & Weaver, T. A. 1995, ApJS, 98, 617
Todt, H., Sander, A., Hainich, R., et al. 2015, A&A, 579, A75
Vanbeveren, D. & Conti, P. S. 1980, A&A, 88, 230
Venn, K. A. 1999, ApJ, 518, 405
Villaseñor, J. I., Sana, H., Mahy, L., et al. 2025, A&A, 698, A41
Vink, J. S. 2023, A&A, 679, L9
Vink, J. S. & Harries, T. J. 2017, A&A, 603, A120
Wang, C., Patrick, L., Schootemeijer, A., et al. 2025, ApJ, 981, L16
Wang, S. & Chen, X. 2019, ApJ, 877, 116
Weisz, D. R., Dolphin, A. E., Savino, A., et al. 2024, ApJS, 271, 47
Westmoquette, M. S., James, B., Monreal-Ibero, A., & Walsh, J. R. 2013, A&A, 550, A88

Wolf, C., Onken, C. A., Luvaul, L. C., et al. 2018, PASA, 35, e010
Yang, M., Bonanos, A. Z., Jiang, B., et al. 2023, A&A, 676, A84
Yang, M., Bonanos, A. Z., Jiang, B.-W., et al. 2019, A&A, 629, A91
Yang, M., Bonanos, A. Z., Jiang, B.-W., et al. 2018, A&A, 616, A175
Zapartas, E., de Wit, S., Antoniadis, K., et al. 2025, A&A, 697, A167
Zaritsky, D., Kennicutt, Jr., R. C., & Huchra, J. P. 1994, ApJ, 420, 87

Appendix A: Numbers of stars and estimated star-formation rates

In Table A.1, we compile literature SFRs of the galaxies discussed in this study. From there, we can estimate the theoretically expected number of helium-burning stars based on the literature SFR ($N_{\rm HeB,\,lit.\,SFR}$) in the luminosity range $5.0 < \log(L/L_{\odot}) < 5.6$ as follows. We first notice that during helium burning this luminosity range corresponds to initial masses in the range $16 \leq M_{\rm ini}/M_{\odot} \leq 32$. Then we follow the method described in appendix C of Schootemeijer et al. (2021). There, the initial mass function of Kroupa (2001) is integrated to calculate the fraction of stars born in the initial mass range of interest, and their average mass. Then, we look up average lifetimes for stellar models (Schootemeijer et al. 2019) in that mass range, and the typical fraction of their lifetime they spend burning helium (7%). With this information we are able to roughly estimate the relation between the number of helium burning stars in the range $5.0 < \log(L/L_{\odot}) < 5.6$ and the SFR their host galaxy as

$$N_{\rm HeB,\,lit.\,SFR} \approx 1500\,{\rm M}_{\odot}^{-1}\,{\rm yr}. \tag{A.1}$$

For comparison, per galaxy we also provide the observed numbers of cool SGs, $N_{\rm cSG,\,obs}$, in the same luminosity range (Sect. 4.2). In addition to this, we use Eq. A.1 to calculate the minimum constant SFR, $\rm SFR_{min}$, associated with the observed numbers of cool SGs. We emphasize that these are minimum values, because stars can also burn helium as hotter objects (e.g., warm SGs and helium stars), and therefore comparisons with literature SFRs should be performed prudently.

Finally, for the highest-luminosity end ($\log(L/L_{\odot}) > 5.6$), Table A.1 provides: i), the number of cool SGs we predicted in Sect 4.2 based on BoOST models and the number of dimmer cool SGs, ii), the observed number of cool SGs (same references as the other $N_{\rm cSG,\,obs}$ column), and, iii), a brief note on the number of WR stars from literature.

While this table is mainly meant for future reference, we briefly describe a few noticeable features in it. Our values for $\rm SFR_{min}$ are usually somewhat below the literature SFRs, as is to be expected. However, in some cases the values of $\rm SFR_{min}$ are rather far below the literature SFRs, in particular for I Zw 18 and M 31. For I Zw, this difference can be attributed to uncertainties in cool SG lifetimes at extremely low metallicity (see the last paragraph of Sect. 5.4.2). Also, because we inferred the presence of about as much warm SGs as cool SGs in the luminosity range $5.0 < \log(L/L_{\odot}) < 5.6$ in I Zw 18, it is likely that it is forming stars at a rate of at least ~$0.04\,{\rm M}_{\odot}\,{\rm yr}^{-1}$. For M 31, the difference could be caused by relatively short cool SG lifetimes, for example because stars evolve into low-luminosity WR stars ($5.0 < \log(L/L_{\odot}) < 5.6$) or intermediate-temperature objects. According to McDonald et al. (2022), their sample is rather complete, which would disqualify completeness issues as a cause for the low number of cool SGs observed in M 31. Finally, based on the number of cool SGs at ($5.0 < \log(L/L_{\odot}) < 5.6$) in the SMC, we would expect as much as 32 cool SGs or other helium-burning objects at $\log(L/L_{\odot}) > 5.6$. However, in this luminosity range there are at most 11 WR stars, and objects with temperatures between those of cool SGs and main-sequence stars seem to be no more than a handful in number (Blaha & Humphreys 1989; Massey et al. 1995; Schootemeijer et al. 2021). As such, about half of the expected helium-burning stars are missing at $\log(L/L_{\odot}) > 5.6$. Possible explanations could have to do with one or more of the following: a recent decrease in SFR of the order of 50%; a steeper initial mass function; or stars burning helium at temperatures that overlap with the main sequence.

Table A.1. Numbers of certain types of stars and star formation rates in different galaxies.

Galaxy	SFR (lit.) $[M_\odot\,yr^{-1}]$	$N_{HeB,\,lit.\,SFR}$ (5<logL<5.6)	$N_{cSG,\,obs}$ (5<logL<5.6)	SFR_{min} $[M_\odot\,yr^{-1}]$	$N_{cSG,\,pred}$ (logL>5.6)	$N_{cSG,\,obs}$ (logL>5.6)	$N_{WR,\,obs}$ (logL>5.6)
I Zw 18	0.1-1	150-1500	28	0.019	90 (10[a)])	0	'tens' (estimated, no L provided)
SMC	0.05	75	41[c)]	0.027	32	0	11 (3 can be H-burning[b)])
NGC 5253	0.1, 0.2	150, 300	71	0.047	52	1	30 to 40 (estimated, no L provided)
LMC	0.2	300	72[c)]	0.048	21	1	~80 (half can be H-burning[b)])
NGC 300	0.08-0.16	120-240	86	0.057	21	0	30 to 40 (estimated, no L provided)
NGC 4395	0.03, 0.5	45, 750	86	0.057	19	0	'WR features'
M 31	0.7	1050	117[d)]	0.078			

Notes. The text in Appendix A describes how these numbers and the minimum star formation rate are obtained. Explanation of notes in the table: [a)]: if, instead, a constant cool SG lifetime fraction of 7% of the stellar lifetime is assumed – [b)]: these stars can be hydrogen burning because they have temperatures lower than the zero-age main-sequence temperature. – [c)]: from Davies et al. (2018) – [d)]: from McDonald et al. (2022). Literature SFR references: I Zw 18: table 1 of Hirschauer et al. (2024), Bortolini et al. (2024); SMC: Harris & Zaritsky (2004); N5253: López-Sánchez et al. (2012); LMC: Harris & Zaritsky (2009); N300: Helou et al. (2004), Kang et al. (2025); N4395: Smirnova et al. (2020), Nandi et al. (2023); M31: Lewis et al. (2015). References for $N_{WR,\,obs}$: Sect. 5.3.4, Hainich et al. (2014, 2015) for LMC and SMC, respectively.